Coupled pitching dynamics of flexible space structures with on-board liquid sloshing

Coupled pitching dynamics of flexible space structures with on-board liquid sloshing

M. Chiba [a,*], H. Magata [a]

[a] *Department of Aerospace Engineering, Graduate School of Engineering, Osaka Prefecture University, 1-1 Gakuen-cho, Nakaku, Sakai, Osaka 599-8531, Japan*

[*]Corresponding author. Tel/Fax: +81 72 254 9235 *E-mail address: chiba@aero.osakafu-u.ac.jp (M. Chiba)*

Abstract

In this study, we analyzed the influence of liquid sloshing on the pitching dynamics of flexible space structure with liquid on board; the analysis considers the main body of a spacecraft as a rigid tank, the flexible appendages as two elastically supported elastic beams, and on-board liquid as an ideal liquid. The meniscus of the free surface of the liquid due to surface tension was considered. The Lagrangians of the main body of the spacecraft (rigid tank), liquid, and two beams (flexible appendages) were used in addition to assuming antisymmetric motion of the system; the frequency equations of the coupled system were obtained by applying the *Rayleigh–Ritz* method. Influence of moment of inertia of the main body on coupled motions of the flexible spacecraft was investigated.

Keywords: pitching dynamics, flexible space structures, coupled system, Rayleigh-Ritz method

1. Introduction

Large space structures vibrate easily at low frequencies because they possess low structural rigidity, given their requirement to be lightweight. Attitude control or orbit modification through thruster injection could cause flexible appendages such as antennae and solar arrays, as well as the liquid fuel or wastewater on the spacecraft, to vibrate and develop strong coupled vibrations that exert a complex effect on the dynamic behavior of the main body. This poses a serious problem for high-attitude-accuracy satellites such as those used for precise astronomical photography. Therefore, it is essential to clarify the dynamic interaction behavior of a flexible space structure with on-board liquid, in advance of its deployment, to improve the stability and reliability of space structures.

Several researchers have examined the sloshing of liquids in containers in low-gravity environments theoretically. For example, Abramson [1] conducted a review of studies up until 1966. Bauer et al. [2, 3] studied free vibration analyses of a liquid in a cylindrical or rectangular vessel taking into consideration the liquid

meniscus due to surface tension. Agrawal [4] analyzed the dynamic behavior of liquid in a rotating space vehicle using a boundary-layer model. Komatsu [5] theoretically investigated the sloshing frequency in a space vehicle tank using a mechanical model and used potential flow models to obtain natural frequencies via a semi-empirical formula. Chiba et al. [6] investigated the coupled natural vibration of an elastic membrane bottom and liquid in a cylindrical container with a rigid wall. Utsumi [7] proposed mechanical models for sloshing in a tear-shaped axisymmetric tank. Yuajun [8] carried out a nonlinear analysis of liquid sloshing in a cylindrical container considering the static meniscus shape in low-gravity environments using an energy method under pitching excitation around the center of gravity of the cylinder. Berglund [9] controlled the sloshing of liquid propellant in a Delta IV rocket using a pulse-suppression approach. Cui et al. [10] studied parametric instability of liquid sloshing in a spacecraft model during launch. Noorian et al. [11] studied coupled dynamics of fuel contained elastic launch vehicles using a BEM-FEM model.

However, few experimental studies have focused on resolving the sloshing that occurs in low-gravity environments. The Netherlands Agency for Aerospace (NIVR) launched a 130 kg miniature satellite called "Sloshsat Flevo" with an 87 *l* tank, which contained 33.5 *l* of water, to investigate the effect of sloshing behavior on the motion of the satellite, see Vreeburg [12]. Lazzarin et al. [13] estimated the impact of propellant sloshing on the pointing stability of the EUCLID satellite by CFD simulation.

Additionally, with respect to the effects of sloshing on spacecraft motion, the relationship between the balance and stability of a flat, rotating spacecraft with liquid fuel on-board was revealed by McIntyre et al. [14]. Santini et al. [15, 16] derived equations of motion of orbiting spacecraft with a sloshing liquid in a plane rigid tank and discussed its stability. Lü et al. [17] studied pitching motion of a two-dimensional rectangular tank with elastic appendages under gravity. From the numerical simulations, they found that the coupling of elastic appendages with rigid tanks are effective in high-gravity conditions, while the coupling of liquid fuel and rigid tanks are effective in low-gravity conditions. Recently, Farhat et al. [18] investigated the effect of fuel sloshing on a spacecraft and its flutter characteristics. Gasbarri et al. [19] presented a dynamic model of spacecraft with a solar panel and considered fuel sloshing using a multibody approach. They employed a pendulum model for the fuel sloshing and clarified the interaction among the control, the attitude dynamics, the flexibility of the solar array, and the sloshing motion of the spacecraft. For spacecraft with multiple propellant tanks, Baozeng et al. [20] presented a coupled dynamic model using Lagrange's equation, and Zhou and Huang [21] presented a constrained surface model in which they clarified the coupling dynamics between the spacecraft and the propellant sloshing in tanks.

A recent study constituted the initial step in clarifying the fundamental vibration characteristics of flexible space structures with on-board liquid, by proposing a mechanical model, and theoretically analyzing the axisymmetric coupled vibrations of a flexible structure with on-board liquid in zero-gravity environments (Chiba et al. [22]). The proposed model involved modelling the main body as a rigid mass, flexible appendages as two elastic beams, and on-board liquid as a "spring-mass" system (mechanical model). A single liquid sloshing mode (i.e. fundamental sloshing mode) was adopted in the mechanical model, and this helped in determining the fundamental vibration characteristics of the coupled system, i.e. the main body–flexible appendages–liquid system. As the second step, the on-board liquid was modelled as a potential fluid considering a static meniscus of the free surface due to surface tension by Chiba et al. [23]. In addition, the effect of spring rigidity of the flexible appendages was analyzed for the same model by Chiba et al. [24].

The present study follows on from the aforementioned study as the fourth step, additionally analyzing the pitching motion of the spacecraft.

2. Basic equations and boundary conditions

2.1. Analytical model

In the study, free pitching vibrations of a spacecraft in space are considered, as shown in Fig. 1. The spacecraft included flexible appendages, such as solar arrays on both sides of the main body Fig. 1(a) and the liquid fuel on-board (Fig. 1(b)). The main body of the spacecraft is modelled as a rigid tank, flexible appendages as two elastic beams, and on-board liquid as an ideal liquid.

A rigid cylindrical tank with radius R and length H has a mass m_t and moment of inertia J_t; the tank harmonically rotates with a small angle θ around the *Y* axis in the inertia coordinate $O-XYZ$ (Fig. 1(a)). While two beams are modelled as uniform Euler–Bernoulli beams with length l, cross-sectional area A, density ρ_b, mass m_b, Young's modulus E, and second moment of area I, with displacements corresponding to $W_i(x_i, t), i=1, 2$. They are fixed on the tank wall at height e from the tank bottom.

On-board liquid fuel is treated as an inviscid ideal fluid with density ρ_f and mass $m_f=\pi R^2 h\rho_f$, where h denotes liquid height when the meniscus of the liquid is ignored. The velocity potential of the liquid $\Phi(r, \varphi, z, t)$ is introduced into the coordinate system $O-r\varphi z$, in which the origin is considered to be located on a flat liquid surface, and the moment of inertia of the liquid is J_f. In a zero-gravity condition, the surface tension σ is predominant on the liquid, which produces an axisymmetric meniscus $z_0(r)$, as shown

Nomenclature

A	Cross-sectional area of beam	R	Radius of rigid tank
E	Young's modulus of beam	$S(r, \varphi, t)$: (ζ)	Amplitude of liquid surface :($\zeta = S / R$)
e: ($\bar{e}$)	Distance between tank bottom and center of gravity	t	Time: $(\tau = \omega_b t)$
H : ($\bar{H}$)	Height of tank	W_i : (w_i)	Displacements of beams :($w_i = W_i / l$)
h : (h_0)	Equivalent liquid height :$(h_0 = h / R)$	$z_0(r)$: (η_0)	Static liquid free surface :($\eta_0 = z_0 / R$)
I	Moment of inertia of area of beam	θ	Rotation angle
J_f : ($\bar{J}_f$)	Moment of inertia of liquid	θ_0	Static contact angle of liquid
J_t : ($\bar{J}_t$)	Moment of inertia of tank	ξ_i	Non-dimensional coordinate :($= x_i / l$)
l	Length of beam $(\lambda = l/R)$	ρ_b	Density of beam
m_t : ($\bar{m}_t$)	Mass of rigid tank	ρ_f : ($\bar{\rho}$)	Density of liquid
m_b	Mass of beam	σ : (γ)	Coefficient of free surface tension
$O-XYZ$	Inertial coordinate system for spacecraft	$\Phi(r, \varphi, z, t)$: (ϕ)	Liquid velocity potential :($\phi = \Phi / \omega_b R^2$)
$O-xyz$	Coordinate system for tank	ω:(Ω)	Coupled natural circular frequency ($\Omega = \omega/\omega_b$)
$o_i - x_i y_i z_i$	Coordinate system for beam i	ω_b	Natural circular frequency of beam ($= \sqrt{EI/\rho_b A l^4}$)
$O-r\varphi z$	Coordinate system for liquid		

in Fig. 1(b), with contact angle θ_0 with respect to a side wall. Therefore, the free surface of the liquid vibrates with amplitude $S(r,\varphi,t)$ around the meniscus.

It is assumed that the two beams are arranged symmetrically with respect to the rigid tank, and that the mass center of the rigid tank is located on the mid-surface of the beams. This enabled antisymmetric in-plane motion, i.e., movement along only the clockwise and counterclockwise directions in the plane of the figure.

2.2. Basic equations and boundary conditions

2.2.1. Basic equations and boundary conditions for liquid

It is assumed that the liquid is incompressible, inviscid, and exhibits irrotational motion, based on which there exists a velocity potential of the liquid $\phi(\rho, \varphi, \eta, \tau)$ in non-dimensional form that satisfies the Laplace equation as follows:

$$\frac{\partial^2 \phi}{\partial \rho^2} + \frac{1}{\rho}\frac{\partial \phi}{\partial \rho} + \frac{1}{\rho^2}\frac{\partial^2 \phi}{\partial \varphi^2} + \frac{\partial^2 \phi}{\partial \eta^2} = 0 \tag{1}$$

Velocity components of velocity $\mathbf{v}_c$, v_ρ, v_φ, v_η induced by pitching motion of the rigid tank are represented as: see Kimura et al. [25].

$$\boldsymbol{v}_c = v_\rho \boldsymbol{e}_\rho + v_\varphi \boldsymbol{e}_\varphi + v_\eta \boldsymbol{e}_\eta \qquad \begin{cases} v_\rho = -d\theta / d\tau \, \eta \cos\varphi \\ v_\varphi = d\theta / d\tau \, \eta \sin\varphi \\ v_\eta = d\theta / d\tau \, \rho \cos\varphi \end{cases} \tag{2}$$

where $\boldsymbol{e}_\rho$, $\boldsymbol{e}_\varphi$, $\boldsymbol{e}_\eta$ are basic vectors for ρ, φ, η directions, respectively. The dynamic condition on the free surface is as follows (Bauer et al. [2]):

$$\frac{\partial \phi}{\partial \tau} - \frac{\gamma \lambda^3}{\bar{\rho}} \left[\frac{1}{\rho} \frac{\partial}{\partial \rho} \left\{ \rho \left[1 - \left(\rho \cos\theta_0 \right)^2 \right]^{\frac{3}{2}} \frac{\partial \zeta}{\partial \rho} \right\} + \frac{1}{\rho^2} \sqrt{1 - \left(\rho \cos\theta_0 \right)^2} \, \frac{\partial^2 \zeta}{\partial \varphi^2} \right] = 0 \tag{3}$$

$$at \qquad \eta = h_0 - \bar{e} + \eta_0 \left(\rho \right) + \zeta \left(\rho, \varphi, \tau \right)$$

The kinematic condition must be satisfied on the free surface as follows (see Kimura et al. [25]):

$$\frac{\partial \zeta}{\partial \tau} = -\frac{\partial \eta_0 \left(\rho \right)}{\partial \rho} \left\{ \frac{\partial \phi}{\partial \rho} - v_\rho \right\} + \frac{\partial \phi}{\partial \eta} - v_\eta \qquad at \quad \eta = h_0 - \bar{e} + \eta_0 \left(\rho \right) + \zeta \left(\rho, \varphi, \tau \right) \tag{4}$$

At the side wall and the bottom surface of the tank, the following velocity-matching conditions must be satisfied.

$$\left. \frac{\partial \phi}{\partial \rho} \right|_{\rho=1} = v_\rho \tag{5}$$

$$\left. \frac{\partial \phi}{\partial \eta} \right|_{\eta=-\bar{e}} = v_\eta \tag{6}$$

The conservation of liquid volume is represented as follows:

$$\int_0^{2\pi} \int_0^1 \zeta \left(\rho, \varphi, \tau \right) \rho d\rho d\varphi = 0 \tag{7}$$

The meniscus of the free surface of the liquid, caused by surface tension, is represented by Bauer et al. [2] as a function of the contact angle θ_0 with respect to the side walls of the tank using the following expression:

$$\eta_0 \left(\rho \right) = \frac{2\left(1 - \sin^3 \theta_0 \right)}{3\cos^3 \theta_0} - \frac{1}{\cos\theta_0} \sqrt{1 - \left(\rho \cos\theta_0 \right)^2} + h_0 - \bar{e} \tag{8}$$

Here we assume that the contact angle θ_0 does not change during vibrations.

$$\left. \frac{\partial \zeta}{\partial \rho} \right|_{\rho=1} = 0 \tag{9}$$

2.2.2. Basic equations and boundary conditions of the rigid tank and elastic beams

Considering reaction forces and moments from the elastic beams, the moment equilibrium equation in the

rigid tank is given as (see Appendix A):

$$-\bar{J}_t \frac{d^2\theta(\tau)}{d\tau^2} + 2\left(\bar{M}_1 + \frac{1}{\lambda}\bar{R}_1\right) = 0 \tag{10}$$

Next, the equation of motion of the beam is given as:

$$\frac{\partial^2 w_1(\xi_1,\tau)}{\partial\tau^2} + \frac{\partial^4 w_1(\xi_1,\tau)}{\partial\xi_1^4} = 0 \tag{11}$$

Assuming the rotation angle θ is small, the boundary conditions are given as:

at $\xi_1 = 0$ Deflection
$$w_1(0,\tau) = \frac{1}{\lambda}\theta \tag{12}$$

Slope
$$\left.\frac{\partial w_1(\xi_1,\tau)}{\partial\xi_1}\right|_{\xi_1=0} = \theta \tag{13}$$

Bending moment
$$\left.\frac{\partial^2 w_1(\xi_1,\tau)}{\partial\xi_1^2}\right|_{\xi_1=0} = \bar{M}_1 \tag{14}$$

Shearing force
$$-\left.\frac{\partial^3 w_1(\xi_1,\tau)}{\partial\xi_1^3}\right|_{\xi_1=0} = \bar{R}_1 \tag{15}$$

at $\xi_1 = 1$ Bending moment
$$\left.\frac{\partial^2 w_1(\xi_1,\tau)}{\partial\xi_1^2}\right|_{\xi_1=1} = 0 \tag{16}$$

Searing force
$$-\left.\frac{\partial^3 w_1(\xi_1,\tau)}{\partial\xi_1^3}\right|_{\xi_1=1} = 0 \tag{17}$$

2.3. Lagrangian

In this section, we consider the Lagrangian of the liquid, beams, and the main body (tank).

2.3.1. Lagrangian of liquid

The Lagrangian of the liquid $\bar{L}_f$ is represented as a summation of the kinetic energy of the liquid due to rigid tank motions and the dynamic term that was introduced by Luke [26], as follows:

$$\bar{L}_f = \frac{\bar{\beta}\bar{\rho}}{\lambda^3}\bar{J}_f\left(\frac{d\theta}{d\tau}\right)^2 + \frac{2\bar{\beta}}{\pi}\int_0^{2\pi}\int_0^1\left\{\frac{\bar{\rho}}{\lambda^3}\frac{\partial\phi}{\partial\tau} - \gamma\left[\begin{array}{c}\frac{1}{\rho}\frac{\partial}{\partial\rho}\left\{\rho\left[1-\left(\rho\cos\theta_0\right)^2\right]^{\frac{3}{2}}\frac{\partial\zeta}{\partial\rho}\right\} \\ +\frac{1}{\rho^2}\sqrt{1-\left(\rho\cos\theta_0\right)^2}\,\frac{\partial^2\zeta}{\partial\varphi^2}\end{array}\right]\right\}\zeta\rho d\rho d\varphi \tag{18}$$

where $\bar{J}_f$ is the moment of inertia of the liquid in the tank and details are shown in Appendix C.

2.3.2. Lagrangian of the beams and the main body (tank)

The Lagrangian of the beams and the main body (tank) comprise kinetic energy $\bar{T}$ and potential energy $\bar{U}$; it is expressed as follows:

$$\begin{aligned}\bar{L}_{tb} &= \bar{T} - \bar{U} \\ &= \int_0^1 \left(\frac{\partial w_1}{\partial \tau}\right)^2 d\xi_1 + \frac{1}{2}\bar{J}_t \left(\frac{d\theta}{d\tau}\right)^2 - \int_0^1 \left(\frac{\partial^2 w_1}{\partial \xi_1^2}\right)^2 d\xi_1\end{aligned} \tag{19}$$

where two beams are assumed to be identical.

In the above equations, we introduced the following non-dimensional parameters as given below:

$$\begin{aligned}&\tau = \omega_b t,\ \omega_b = \sqrt{\frac{EI}{\rho_b A l^4}},\ \Omega = \frac{\omega}{\omega_b},\ \rho = \frac{r}{R},\ \phi = \frac{\Phi}{\omega_b R^2},\ \eta = \frac{z}{R},\ \eta_0 = \frac{z_0}{R},\ \zeta = \frac{S}{R},\ \gamma = \frac{\sigma A l}{EI}, \\ &h_0 = \frac{h}{R},\ \bar{\rho} = \frac{\rho_f}{\rho_b},\ \bar{J}_f = \frac{J_f}{\rho_f \pi R^5},\ \lambda = \frac{l}{R},\ \bar{\beta} = \frac{\pi R^2}{2A},\ \bar{e} = \frac{e}{R},\ \xi_i = \frac{x_i}{l},\ \bar{J}_t = \frac{J_t}{\rho_b A l^3},\ w_i = \frac{W_i}{l}, \\ &\bar{H} = \frac{H}{R},\ \bar{m}_t = \frac{m_t}{2m_b},\ \bar{R}_1 = \frac{R_1}{\rho_b A l^2 \omega_b^2},\ \bar{M}_1 = \frac{M_1}{\rho_b A l^3 \omega_b^2},\ v_\rho = \frac{V_r}{\omega_b R} = -\theta_{,\tau}\,\eta\cos\varphi, \\ &v_\varphi = \frac{V_\varphi}{\omega_b R} = \theta_{,\tau}\,\eta\sin\varphi,\ v_\eta = \frac{V_z}{\omega_b R} = \theta_{,\tau}\,\rho\cos\varphi,\ \bar{L}_f = \frac{L_f}{\rho_b \omega_b^2 A l^3},\ \bar{L}_{tb} = \frac{L_{tb}}{\rho_b \omega_b^2 A l^3}\end{aligned} \tag{20}$$

In the above parameters, the moment of inertia of the tank $\bar{J}_t$, ratio of length of the elastic beam and tank radius λ are important parameters, and there is a relation between derivatives with time *t* and with non-dimensional time τ, as:

$$\frac{dk}{dt} = \frac{dk}{d(\tau/\omega_b)} = \omega_b \frac{dk}{d\tau} \tag{21}$$

3. Method of solution

3.1. Elimination of temporal terms

It is assumed that the system undergoes small-amplitude harmonic motion with the circular frequency Ω as follows:

$$\begin{aligned}&\theta(\tau) = \bar{\theta}\cos\Omega\tau \\ &\phi(\rho,\varphi,\eta,\tau) = -\Omega\bar{\phi}(\rho,\varphi,\eta)\sin\Omega\tau \\ &\zeta(\rho,\varphi,\tau) = \bar{\zeta}(\rho,\varphi)\cos\Omega\tau \\ &w_i(\xi_i,\tau) = \bar{w}_i(\xi_i)\cos\Omega\tau \\ &\bar{R}_1(\tau) = \tilde{R}_1\cos\Omega\tau \\ &\bar{M}_1(\tau) = \tilde{M}_1\cos\Omega\tau\end{aligned} \tag{22}$$

3.1.1. Equations and boundary conditions for liquid

Substituting the above equation into Eq. (1) to Eq. (9), we obtain as: In the following equations, non-dimensional velocities v_ρ, v_φ, v_η are represented in terms of pitching angle θ:

$$\frac{\partial^2\bar{\phi}}{\partial\rho^2}+\frac{1}{\rho}\frac{\partial\bar{\phi}}{\partial\rho}+\frac{1}{\rho^2}\frac{\partial^2\bar{\phi}}{\partial\varphi^2}+\frac{\partial^2\bar{\phi}}{\partial\eta^2}=0 \tag{1}'$$

$$\Omega^2\bar{\phi}\left(\rho,\varphi,\eta\right)+\frac{\gamma\lambda^3}{\bar{\rho}}\left[\frac{1}{\rho}\frac{\partial}{\partial\rho}\left\{\rho\left[1-\left(\rho\cos\theta_0\right)^2\right]^{\frac{3}{2}}\frac{\partial\bar{\zeta}\left(\rho,\varphi\right)}{\partial\rho}\right\}+\frac{1}{\rho^2}\sqrt{1-\left(\rho\cos\theta_0\right)^2}\,\frac{\partial^2\bar{\zeta}\left(\rho,\varphi\right)}{\partial\varphi^2}\right]=0 \tag{3}'$$

$$at \quad \eta=h_0-\bar{e}+\eta_0\left(\rho\right)$$

$$\bar{\zeta}\left(\rho,\varphi\right)+\frac{\partial\eta_0\left(\rho\right)}{\partial\rho}\frac{\partial\bar{\phi}}{\partial\rho}+\bar{\theta}\frac{\partial\eta_0\left(\rho\right)}{\partial\rho}\eta\cos\varphi-\frac{\partial\bar{\phi}}{\partial\eta}+\bar{\theta}\rho\cos\varphi=0 \qquad at \quad \eta=h_0-\bar{e}+\eta_0\left(\rho\right) \tag{4}'$$

$$\left.\frac{\partial\bar{\phi}\left(\rho,\varphi,\eta\right)}{\partial\rho}\right|_{\rho=1}=-\bar{\theta}\eta\cos\varphi \tag{5}'$$

$$\left.\frac{\partial\bar{\phi}\left(\rho,\varphi,\eta\right)}{\partial\eta}\right|_{\eta=-\bar{e}}=\bar{\theta}\rho\cos\varphi \tag{6}'$$

$$\int_0^{2\pi}\int_0^1\bar{\zeta}\left(\rho,\varphi\right)\rho d\rho d\varphi=0 \tag{7}'$$

$$\left.\frac{\partial\bar{\zeta}}{\partial\rho}\right|_{\rho=1}=0 \tag{9}'$$

3.1.2. Equations and boundary condition for rigid tank and elastic beams

$$\bar{J}_t\Omega^2\bar{\theta}+2\left(\tilde{M}_1+\frac{1}{\lambda}\tilde{R}_1\right)=0 \tag{10}'$$

$$\Omega^2\bar{w}_i\left(\xi_i\right)-\frac{\partial^4\bar{w}_1\left(\xi_1\right)}{\partial\xi_1^{\,4}}=0 \tag{11}'$$

at $\xi_1=0$ Deflection $$\bar{w}_i\left(0\right)=\frac{1}{\lambda}\bar{\theta} \tag{12}'$$

Slope $$\left.\frac{\partial\bar{w}_i\left(\xi_i\right)}{\partial\xi_1}\right|_{\xi_1=0}=\bar{\theta} \tag{13}'$$

Bending moment $$\left.\frac{\partial^2\bar{w}_1\left(\xi_1\right)}{\partial\xi_1^{\,2}}\right|_{\xi_1=0}=\tilde{M}_1 \tag{14}'$$

Shearing force $$-\left.\frac{\partial^3 \bar{w}_i(\xi_i)}{\partial \xi_1^{\,3}}\right|_{\xi_1=0} = \tilde{R}_1 \qquad (15)'$$

at $\xi_1 = 1$ Bending moment $$\left.\frac{\partial^2 \bar{w}_1(\xi_1)}{\partial \xi_1^2}\right|_{\xi_1=1} = 0 \qquad (16)'$$

Searing force $$-\left.\frac{\partial^3 \bar{w}_1(\xi_1)}{\partial \xi_1^3}\right|_{\xi_1=1} = 0 \qquad (17)'$$

3.1.3. Lagrangian for liquid

$$\tilde{L}_f = \frac{\bar{\beta}\bar{\rho}}{\lambda^3}\bar{J}_f\Omega^2\bar{\theta}^2 - \frac{2\bar{\beta}}{\pi}\int_0^{2\pi}\int_0^1 \left\{ \Omega^2 \frac{\bar{\rho}}{\lambda^3}\bar{\phi} + \gamma \left[\begin{array}{l} \dfrac{1}{\rho}\dfrac{\partial}{\partial\rho}\left\{\rho\left[1-(\rho\cos\theta_0)^2\right]^{\frac{3}{2}}\dfrac{\partial\bar{\zeta}}{\partial\rho}\right\} \\ +\dfrac{1}{\rho^2}\sqrt{1-(\rho\cos\theta_0)^2}\,\dfrac{\partial^2\bar{\zeta}}{\partial\varphi^2} \end{array} \right] \right\} \bar{\zeta}\,\rho d\rho d\varphi \qquad (18)'$$

where we used the relations:

$$\tilde{L}_f = \frac{\Omega}{\pi}\int_0^{2\pi/\Omega}\bar{L}_f d\tau \qquad (23)$$

$$\int_0^{2\pi/\Omega}\sin^2\Omega\tau d\tau = \int_0^{2\pi/\Omega}\cos^2\Omega\tau d\tau = \frac{\pi}{\Omega} \qquad (24)$$

3.1.4. Lagrangian for rigid tank and elastic beams

$$\tilde{L}_{tb} = \Omega^2\int_0^1 \bar{w}_1{}^2(\xi_1)\,d\xi_1 + \frac{\Omega^2}{2}\bar{J}_t\bar{\theta}^2 - \int_0^1\left(\frac{\partial^2\bar{w}_1}{\partial\xi_1^2}\right)^2 d\xi_1 \qquad (19)'$$

where we used the following equation and Eq. (24):

$$\tilde{L}_{tb} = \frac{\Omega}{\pi}\int_0^{2\pi/\Omega}\bar{L}_{tb}d\tau \qquad (25)$$

3.2. Velocity potential of liquid

The liquid velocity potential that satisfies the Laplace equation (1)' and the boundary conditions in Eq. (5)' to Eq. (7)', and Eq. (9)', and the displacement of a free surface are assumed in the following form:

$$\bar{\phi}(\rho,\varphi,\eta) = \sum_n A_{mn}J_m(\varepsilon_{mn}\rho)\cos m\varphi\frac{\cosh\{\varepsilon_{mn}(\eta+\bar{e})\}}{\cosh(\varepsilon_{mn}h_0)} + 4\bar{\theta}\cos\varphi\sum_i\frac{J_1(\varepsilon_{1i}\rho)\sinh(\varepsilon_{1i}\eta)}{\varepsilon_{1i}\left(\varepsilon_{1i}{}^2-1\right)J_1(\varepsilon_{1i})\cosh(\varepsilon_{1i}\bar{e})} - \bar{\theta}\rho\eta\cos\varphi \qquad (26)$$

$$\bar{\zeta}(\rho,\varphi)=\sum_n a_{mn}J_m(\varepsilon_{mn}\rho)\cos m\varphi \tag{27}$$

where A_{mn} and a_{mn} are unknown constants. Substituting these equations into Eq. (4)', we obtain:

$$\begin{aligned}&\sum_n a_{mn}J_m(\varepsilon_{mn}\rho)\cos m\varphi+\frac{\partial\eta_0(\rho)}{\partial\rho}\sum_n A_{mn}\cos m\varphi\frac{dJ_m(\varepsilon_{mn}\rho)}{d\rho}\frac{\cosh\{\varepsilon_{mn}(\eta+\bar{e})\}}{\cosh(\varepsilon_{mn}h_0)}\\&+\frac{\partial\eta_0(\rho)}{\partial\rho}\sum_i\frac{dJ_1(\varepsilon_{1i}\rho)}{d\rho}\frac{4\bar{\theta}\cos\varphi\sinh(\varepsilon_{1i}\eta)}{\varepsilon_{1i}\left({\varepsilon_{1i}}^2-1\right)J_1(\varepsilon_{1i})\cosh(\varepsilon_{1i}\bar{e})}+2\bar{\theta}\rho\cos\varphi\\&-\sum_n A_{mn}J_m(\varepsilon_{mn}\rho)\varepsilon_{mn}\cos m\varphi\frac{\sinh\{\varepsilon_{mn}(\eta+\bar{e})\}}{\cosh(\varepsilon_{mn}h_0)}-4\bar{\theta}\varepsilon_{1i}\cos\varphi\sum_i\frac{J_1(\varepsilon_{1i}\rho)\cosh(\varepsilon_{1i}\eta)}{\varepsilon_{1i}\left({\varepsilon_{1i}}^2-1\right)J_1(\varepsilon_{1i})\cosh(\varepsilon_{1i}\bar{e})}=0\\&\qquad\qquad at\quad \eta=h_0-\bar{e}+\eta_0(\rho)\end{aligned} \tag{28}$$

Multiplying $\cos\varphi$ to the above equation, and integrating over from 0 to 2π, and multiplying $J_1(\varepsilon_{1q}\rho)\rho$ and integrating from 0 to 1, we obtain:

$$a_{1q}=\sum_n A_{1n}\left(C_{3nq}-C_{1nq}\right)+\bar{\theta}\sum_i\left(C_{4iq}-C_{2iq}\right)-\bar{\theta}X_q \tag{29}$$

where coefficients in Eq. (29) are:

$$\begin{aligned}C_{1nq}&=\frac{1}{\chi_{1q}}\int_0^1\frac{\partial\eta_0(\rho)}{\partial\rho}\frac{dJ_1(\varepsilon_{1n}\rho)}{d\rho}\frac{\cosh\left[\varepsilon_{1n}\{h_0+\eta_0(\rho)\}\right]}{\cosh(\varepsilon_{1n}h_0)}J_1(\varepsilon_{1q}\rho)\rho d\rho\\C_{2iq}&=\frac{1}{\chi_{1q}}\int_0^1\frac{\partial\eta_0(\rho)}{\partial\rho}\frac{dJ_1(\varepsilon_{1i}\rho)}{d\rho}\frac{4\sinh\left[\varepsilon_{1i}\{h_0-\bar{e}+\eta_0(\rho)\}\right]}{\varepsilon_{1i}\left({\varepsilon_{1i}}^2-1\right)J_1(\varepsilon_{1i})\cosh(\varepsilon_{1i}\bar{e})}J_1(\varepsilon_{1q}\rho)\rho d\rho\\C_{3nq}&=\frac{1}{\chi_{1q}}\int_0^1\frac{\varepsilon_{1n}\sinh\left[\varepsilon_{1n}\{h_0+\eta_0(\rho)\}\right]}{\cosh(\varepsilon_{1n}h_0)}J_1(\varepsilon_{1n}\rho)J_1(\varepsilon_{1q}\rho)\rho d\rho\\C_{4iq}&=\frac{1}{\chi_{1q}}\int_0^1\frac{4\cosh\left[\varepsilon_{1i}\{h_0-\bar{e}+\eta_0(\rho)\}\right]}{\left({\varepsilon_{1i}}^2-1\right)J_1(\varepsilon_{1i})\cosh(\varepsilon_{1i}\bar{e})}J_1(\varepsilon_{1i}\rho)J_1(\varepsilon_{1q}\rho)\rho d\rho\\X_q&=\frac{4}{\left(\varepsilon_{1q}^2-1\right)J_1(\varepsilon_{1q})}\end{aligned} \tag{30}$$

In the calculation, the orthogonality of the Bessel function is used as follows:

$$\int_0^1 J_1(\varepsilon_{1n}\rho)J_1(\varepsilon_{1q}\rho)\rho d\rho=\frac{1}{2}\left(1-\frac{1}{\varepsilon_{1q}^2}\right)J_1^2(\varepsilon_{1q})\,\delta_{nq}=\chi_{1q} \tag{31}$$

where δ_{nq} denotes the Kronecker delta.

Substituting liquid velocity Eq. (26) and liquid displacement Eq. (27) into Lagrangian of the liquid, we obtain the following, in which $m=1$ in Eq. (26) and Eq. (27):

$$\tilde{L}_f = \frac{\bar{\beta}\bar{\rho}}{\lambda^3}\bar{J}_f\Omega^2\bar{\theta}^2 - \Omega^2\frac{2\bar{\beta}\bar{\rho}}{\lambda^3}\sum_j a_{1j}\left\{\sum_n A_{1n}C_{5nj} + \bar{\theta}\left(\sum_i C_{6ij} - C_{7j}\right)\right\} + 2\bar{\beta}\gamma\sum_n a_{1n}\sum_j a_{1j}\left(C_{9nj} - C_{8nj}\right) \tag{32}$$

where coefficients in Eq. (32) are:

$$\begin{aligned}
C_{5nj} &= \int_0^1 \frac{\cosh\left[\varepsilon_{1n}\left\{h_0 + \eta_0(\rho)\right\}\right]}{\cosh\left(\varepsilon_{1n}h_0\right)} J_1\left(\varepsilon_{1n}\rho\right) J_1\left(\varepsilon_{1j}\rho\right)\rho d\rho \\
C_{6ij} &= \int_0^1 \frac{4J_1\left(\varepsilon_{1i}\rho\right)\sinh\left[\varepsilon_{1i}\left\{h_0 - \bar{e} + \eta_0(\rho)\right\}\right]}{\varepsilon_{1i}\left({\varepsilon_{1i}}^2 - 1\right)J_1\left(\varepsilon_{1i}\right)\cosh\left(\varepsilon_{1i}\bar{e}\right)} J_1\left(\varepsilon_{1j}\rho\right)\rho d\rho \\
C_{7j} &= \int_0^1 \left\{h_0 - \bar{e} + \eta_0(\rho)\right\} J_1\left(\varepsilon_{1j}\rho\right)\rho^2 d\rho \\
C_{8nj} &= -\int_0^1 \rho\left[1 - \left(\rho\cos\theta_0\right)^2\right]^{\frac{3}{2}} \frac{\partial J_1\left(\varepsilon_{1n}\rho\right)}{\partial\rho}\frac{\partial J_1\left(\varepsilon_{1j}\rho\right)}{\partial\rho} d\rho \\
C_{9nj} &= \int_0^1 \frac{1}{\rho}\sqrt{1 - \left(\rho\cos\theta_0\right)^2} J_1\left(\varepsilon_{1n}\rho\right) J_1\left(\varepsilon_{1j}\rho\right) d\rho
\end{aligned} \tag{33}$$

Substituting Eq. (29) into the second and third terms of the right-hand side of Eq. (32), we obtain:

$$\begin{aligned}
\tilde{L}_f = \frac{\bar{\beta}\bar{\rho}}{\lambda^3}\bar{J}_f\Omega^2\bar{\theta}^2 - \Omega^2\frac{2\bar{\beta}\bar{\rho}}{\lambda^3}\sum_j &\left[\begin{array}{l}
\sum_k A_{1k}\sum_s A_{1s}C_{5sj}\left(C_{3kj} - C_{1kj}\right) + \bar{\theta}^2\left\{\sum_q\left(C_{4qj} - C_{2qj}\right) - X_j\right\}\left(\sum_i C_{6ij} - C_{7j}\right) \\
+ \bar{\theta}\sum_k A_{1k}\left\{\left(C_{3kj} - C_{1kj}\right)\left(\sum_i C_{6ij} - C_{7j}\right) + C_{5kj}\left(\sum_q\left(C_{4qj} - C_{2qj}\right) - X_j\right)\right\}
\end{array}\right] \\
+ 2\bar{\beta}\gamma\sum_n\sum_j\left(C_{9nj} - C_{8nj}\right)&\left[\begin{array}{l}
\sum_k A_{1k}\sum_s A_{1s}\left(C_{3sn} - C_{1sn}\right)\left(C_{3kj} - C_{1kj}\right) \\
+ \bar{\theta}\sum_k A_{1k}\left\{\begin{array}{l}\left(C_{3kn} - C_{1kn}\right)\left(\sum_q\left(C_{4qj} - C_{2qj}\right) - X_j\right) \\ +\left(C_{3kj} - C_{1kj}\right)\left(\sum_p\left(C_{4pn} - C_{2pn}\right) - X_n\right)\end{array}\right\} \\
+ \bar{\theta}^2\left\{\sum_p\left(C_{4pn} - C_{2pn}\right) - X_n\right\}\left\{\sum_q\left(C_{4qj} - C_{2qj}\right) - X_j\right\}
\end{array}\right]
\end{aligned} \tag{34}$$

3.3. Displacement function for beam

Here, the beam displacements are assumed to be in the following form:

$$\bar{w}_1\left(\xi_1\right) = \sum_u B_u\tilde{w}_{1u}\left(\xi_1\right) \tag{35}$$

where B_u denotes the unknown constant, and $\tilde{w}_{iu}\left(\xi_i\right)$: $i = 1, 2$ denotes the eigenfunction of the beam that satisfies the boundary conditions in Eq. (10)' – Eq. (17)', and whose derivation is in Appendix B.

$$\begin{aligned}\tilde{w}_{iu}\left(\xi_i\right)=&\left\{\lambda\sin\alpha_u\cosh\alpha_u-\lambda\cos\alpha_u\sinh\alpha_u+\alpha_u+\alpha_u\cos\alpha_u\cosh\alpha_u+\alpha_u\sin\alpha_u\sinh\alpha_u\right\}\cosh\alpha_u\xi_i\\&+\left\{-\lambda\sin\alpha_u\cosh\alpha_u+\lambda\cos\alpha_u\sinh\alpha_u+\alpha_u+\alpha_u\cos\alpha_u\cosh\alpha_u-\alpha_u\sin\alpha_u\sinh\alpha_u\right\}\cos\alpha_u\xi_i\\&+\left\{\lambda\cos\alpha_u\cosh\alpha_u-\lambda\sin\alpha_u\sinh\alpha_u+\lambda-\alpha_u\cos\alpha_u\sinh\alpha_u-\alpha_u\sin\alpha_u\cosh\alpha_u\right\}\sinh\alpha_u\xi_i\\&+\left\{\lambda\cos\alpha_u\cosh\alpha_u+\lambda\sin\alpha_u\sinh\alpha_u+\lambda+\alpha_u\cos\alpha_u\sinh\alpha_u+\alpha_u\sin\alpha_u\cosh\alpha_u\right\}\sin\alpha_u\xi_i\end{aligned}\tag{36}$$

The parameter α_u satisfies the frequency equation below:

$$\begin{aligned}&2\lambda^2\left(\cosh\alpha_u\sin\alpha_u-\sinh\alpha_u\cos\alpha_u\right)+2\alpha_u^2\left(\cosh\alpha_u\sin\alpha_u+\sinh\alpha_u\cos\alpha_u\right)\\&+4\lambda\alpha_u\sinh\alpha_u\sin\alpha_u+\bar{J}_t\lambda^2\alpha_u^3\cosh\alpha_u\cos\alpha_u+\bar{J}_t\lambda^2\alpha_u^3=0\end{aligned}\tag{37}$$

which is a function of aspect ratio λ and inertia moment $\bar{J}_t$.

Substituting Eq. (35) into the Lagrangian, we obtain the following expression:

$$\tilde{L}_{tb}=\Omega^2\sum_u\sum_v B_uB_v\int_0^1\tilde{w}_{1u}\left(\xi_1\right)\tilde{w}_{1v}\left(\xi_1\right)d\xi_1+\frac{\Omega^2}{2}\bar{J}_t\bar{\theta}^2-\sum_u\sum_v B_uB_v\int_0^1\left(\frac{\partial^2\tilde{w}_{1u}\left(\xi_1\right)}{\partial\xi_1^2}\right)\left(\frac{\partial^2\tilde{w}_{1v}\left(\xi_1\right)}{\partial\xi_1^2}\right)d\xi_1\tag{38}$$

3.4. Lagrangian for the entire system

Finally, the Lagrangian for the entire system is obtained as follows:

$$\tilde{L}=\tilde{L}_f+\tilde{L}_{tb}\tag{39}$$

$$\begin{aligned}\tilde{L}=&\frac{\bar{\beta}\bar{\rho}}{\lambda}\bar{J}_f\Omega^2\sum_u\sum_v B_uB_v\tilde{w}_u\left(0\right)\tilde{w}_v\left(0\right)\\&-\Omega^2\frac{2\bar{\beta}\bar{\rho}}{\lambda^3}\sum_j\left[\begin{array}{l}\sum_k A_{1k}\sum_s A_{1s}C_{5sj}\left(C_{3kj}-C_{1kj}\right)\\+\lambda^2\sum_u\sum_v B_uB_v\tilde{w}_u\left(0\right)\tilde{w}_v\left(0\right)\left\{\sum_q\left(C_{4qj}-C_{2qj}\right)-X_j\right\}\left(\sum_i C_{6ij}-C_{7j}\right)\\+\lambda\sum_u B_u\tilde{w}_u\left(0\right)\sum_k A_{1k}\left\{\left(C_{3kj}-C_{1kj}\right)\left(\sum_i C_{6ij}-C_{7j}\right)+C_{5kj}\left(\sum_q\left(C_{4qj}-C_{2qj}\right)-X_j\right)\right\}\end{array}\right]\\&+2\bar{\beta}\gamma\sum_n\sum_j\left(C_{9nj}-C_{8nj}\right)\left[\begin{array}{l}\sum_k A_{1k}\sum_s A_{1s}\left(C_{3sn}-C_{1sn}\right)\left(C_{3kj}-C_{1kj}\right)\\+\lambda\sum_u B_u\tilde{w}_u\left(0\right)\sum_k A_{1k}\left\{\begin{array}{l}\left(C_{3kn}-C_{1kn}\right)\left(\sum_q\left(C_{4qj}-C_{2qj}\right)-X_j\right)\\+\left(C_{3kj}-C_{1kj}\right)\left(\sum_p\left(C_{4pn}-C_{2pn}\right)-X_n\right)\end{array}\right\}\\+\lambda^2\sum_u\sum_v B_uB_v\tilde{w}_u\left(0\right)\tilde{w}_v\left(0\right)\left\{\sum_p\left(C_{4pn}-C_{2pn}\right)-X_n\right\}\left\{\sum_q\left(C_{4qj}-C_{2qj}\right)-X_j\right\}\end{array}\right]\end{aligned}\tag{40}$$

$$+\Omega^2\sum_u\sum_v B_uB_v\int_0^1\tilde{w}_{1u}(\xi_1)\tilde{w}_{1v}(\xi_1)d\xi_1+\frac{\Omega^2}{2}\lambda^2\bar{J}_t\sum_u\sum_v B_uB_v\tilde{w}_u(0)\tilde{w}_v(0)$$
$$-\sum_u\sum_v B_uB_v\int_0^1\left(\frac{\partial^2\tilde{w}_{1u}(\xi_1)}{\partial\xi_1^2}\right)\left(\frac{\partial^2\tilde{w}_{1v}(\xi_1)}{\partial\xi_1^2}\right)d\xi_1$$

In the above, pitching angle $\bar{\theta}$ can be represented using the boundary condition Eq. (12)' at $\xi_i=0$.

$$\bar{\theta}=\lambda\sum_u B_u\tilde{w}_u(0) \tag{41}$$

3.5. Rayleigh–Ritz method

The Rayleigh–Ritz method is applied here to obtain the following minimalized condition for:

$$\frac{\partial\tilde{L}}{\partial A_{1k}}=0\ ,\ \frac{\partial\tilde{L}}{\partial B_u}=0 \tag{42}$$

$$\frac{\partial\tilde{L}}{\partial A_{1k}}=2\bar{\beta}\gamma\sum_n\sum_j\left(C_{9nj}-C_{8nj}\right)\left[\begin{array}{l}\sum_s A_{1s}\left\{\left(C_{3kj}-C_{1kj}\right)\left(C_{3sn}-C_{1sn}\right)+\left(C_{3sj}-C_{1sj}\right)\left(C_{3kn}-C_{1kn}\right)\right\}\\ +\lambda\sum_u B_u\tilde{w}_u(0)\left\{\begin{array}{l}\left(C_{3kn}-C_{1kn}\right)\left(\sum_q\left(C_{4qj}-C_{2qj}\right)-X_j\right)\\ +\left(C_{3kj}-C_{1kj}\right)\left(\sum_p\left(C_{4pn}-C_{2pn}\right)-X_n\right)\end{array}\right.\end{array}\right]$$
$$-\Omega^2\frac{2\bar{\rho}\bar{\beta}}{\lambda^3}\sum_j\left[\begin{array}{l}\sum_s A_{1s}C_{5sj}\left(C_{3kj}-C_{1kj}\right)+\sum_s A_{1s}C_{5kj}\left(C_{3sj}-C_{1sj}\right)\\ +\lambda\sum_u B_u\tilde{w}_u(0)\left\{\begin{array}{l}\left(C_{3kj}-C_{1kj}\right)\left(\sum_i C_{6ij}-C_{7j}\right)\\ +C_{5kj}\left(\sum_q\left(C_{4qj}-C_{2qj}\right)-X_j\right)\end{array}\right.\end{array}\right]=0 \tag{43}$$

$$\frac{\partial \tilde{L}}{\partial B_u}=\frac{2\bar{\beta}\bar{\rho}}{\lambda}\bar{J}_f\Omega^2\sum_v B_v\tilde{w}_u(0)\tilde{w}_v(0)$$

$$+2\bar{\beta}\gamma\sum_n\sum_j\left(C_{9nj}-C_{8nj}\right)\left[\begin{array}{l}\lambda\tilde{w}_u(0)\sum_k A_{1k}\left\{\begin{array}{l}\left(C_{3kn}-C_{1kn}\right)\left(\sum_q\left(C_{4qj}-C_{2qj}\right)-X_j\right)\\+\left(C_{3kj}-C_{1kj}\right)\left(\sum_p\left(C_{4pn}-C_{2pn}\right)-X_n\right)\end{array}\right\}\\+2\lambda^2\sum_v B_v\tilde{w}_u(0)\tilde{w}_v(0)\left\{\sum_p\left(C_{4pn}-C_{2pn}\right)-X_n\right\}\left\{\sum_q\left(C_{4qj}-C_{2qj}\right)-X_j\right\}\end{array}\right]$$

$$-\Omega^2\frac{2\bar{\beta}\bar{\rho}}{\lambda^3}\sum_j\left[\begin{array}{l}2\lambda^2\sum_v B_v\tilde{w}_u(0)\tilde{w}_v(0)\left\{\sum_q\left(C_{4qj}-C_{2qj}\right)-X_j\right\}\left(\sum_i C_{6ij}-C_{7j}\right)\\+\lambda\tilde{w}_u(0)\sum_k A_{1k}\left\{\left(C_{3kj}-C_{1kj}\right)\left(\sum_i C_{6ij}-C_{7j}\right)+C_{5kj}\left(\sum_q\left(C_{4qj}-C_{2qj}\right)-X_j\right)\right\}\end{array}\right]$$

$$+2\Omega^2\sum_v B_v\int_0^1\tilde{w}_{1u}(\xi_1)\tilde{w}_{1v}(\xi_1)d\xi_1+\Omega^2\lambda^2\bar{J}_t\sum_v B_v\tilde{w}_u(0)\tilde{w}_v(0)$$

$$-2\sum_v B_v\int_0^1\left(\frac{\partial^2\tilde{w}_{1u}(\xi_1)}{\partial\xi_1^2}\right)\left(\frac{\partial^2\tilde{w}_{1v}(\xi_1)}{\partial\xi_1^2}\right)d\xi_1=0 \tag{44}$$

The above equations can be represented in the following matrix form as coupled equations in terms of A_{1s} and B_v:

$$\left[\begin{pmatrix}K_1 & K_2\\ K_3 & K_4\end{pmatrix}-\Omega^2\begin{pmatrix}M_1 & M_2\\ M_3 & M_4\end{pmatrix}\right]\begin{Bmatrix}A_{1s}\\ B_v\end{Bmatrix}=\mathbf{0} \tag{45}$$

where:

$$
\begin{aligned}
K_1 &= \bar{\beta}\gamma \sum_n \sum_j \left(C_{9nj} - C_{8nj}\right)\left\{\left(C_{3kj} - C_{1kj}\right)\left(C_{3sn} - C_{1sn}\right) + \left(C_{3sj} - C_{1sj}\right)\left(C_{3kn} - C_{1kn}\right)\right\} \\
K_2 &= \bar{\beta}\gamma\lambda \tilde{w}_u\left(0\right) \sum_n \sum_j \left(C_{9nj} - C_{8nj}\right)\left\{\begin{array}{l}\left(C_{3kn} - C_{1kn}\right)\left(\sum_q \left(C_{4qj} - C_{2qj}\right) - X_j\right) \\ +\left(C_{3kj} - C_{1kj}\right)\left(\sum_p \left(C_{4pn} - C_{2pn}\right) - X_n\right)\end{array}\right\} \\
K_3 &= \bar{\beta}\gamma\lambda \tilde{w}_u\left(0\right) \sum_n \sum_j \left(C_{9nj} - C_{8nj}\right)\left\{\begin{array}{l}\left(C_{3kn} - C_{1kn}\right)\left(\sum_q \left(C_{4qj} - C_{2qj}\right) - X_j\right) \\ +\left(C_{3kj} - C_{1kj}\right)\left(\sum_p \left(C_{4pn} - C_{2pn}\right) - X_n\right)\end{array}\right\} \\
K_4 &= 2\bar{\beta}\gamma\lambda^2 \tilde{w}_u\left(0\right)\tilde{w}_v\left(0\right) \sum_n \sum_j \left(C_{9nj} - C_{8nj}\right)\left\{\sum_p \left(C_{4pn} - C_{2pn}\right) - X_n\right\}\left\{\sum_q \left(C_{4qj} - C_{2qj}\right) - X_j\right\} \\
&\quad - \int_0^1 \left(\frac{\partial^2 \tilde{w}_{1u}\left(\xi_1\right)}{\partial \xi_1^2}\right)\left(\frac{\partial^2 \tilde{w}_{1v}\left(\xi_1\right)}{\partial \xi_1^2}\right) d\xi_1 \\
M_1 &= \frac{\bar{\rho}\bar{\beta}}{\lambda^3} \sum_j \left\{C_{5sj}\left(C_{3kj} - C_{1kj}\right) + C_{5kj}\left(C_{3sj} - C_{1sj}\right)\right\} \\
M_2 &= \frac{\bar{\rho}\bar{\beta}}{\lambda^2} \tilde{w}_u\left(0\right) \sum_j \left\{\left(C_{3kj} - C_{1kj}\right)\left(\sum_i C_{6ij} - C_{7j}\right) + C_{5kj}\left(\sum_q \left(C_{4qj} - C_{2qj}\right) - X_j\right)\right\} \\
M_3 &= \frac{\bar{\beta}\bar{\rho}}{\lambda^2} \tilde{w}_u\left(0\right) \sum_j \left\{\left(C_{3kj} - C_{1kj}\right)\left(\sum_i C_{6ij} - C_{7j}\right) + C_{5kj}\left(\sum_q \left(C_{4qj} - C_{2qj}\right) - X_j\right)\right\} \\
M_4 &= -\frac{\bar{\beta}\bar{\rho}}{\lambda} \bar{J}_f \tilde{w}_u\left(0\right)\tilde{w}_v\left(0\right) - \int_0^1 \tilde{w}_{1u}\left(\xi_1\right)\tilde{w}_{1v}\left(\xi_1\right) d\xi_1 - \frac{1}{2}\lambda^2 \bar{J}_t \tilde{w}_u\left(0\right)\tilde{w}_v\left(0\right) \\
&\quad + 2\frac{\bar{\beta}\bar{\rho}}{\lambda} \tilde{w}_u\left(0\right)\tilde{w}_v\left(0\right) \sum_j \left\{\sum_q \left(C_{4qj} - C_{2qj}\right) - X_j\right\}\left(\sum_i C_{6ij} - C_{7j}\right)
\end{aligned}
\tag{46}
$$

Thus, the problem can be reduced to an eigenvalue problem, from which the coupled natural circular frequencies Ω can be obtained as eigenvalues and the vibration modes as eigenvectors.

4. Numerical results

The goals of this study included clarifying the influence of liquid sloshing on the coupled hydroelastic pitching vibration characteristics of the flexible space structure. This involved a systematic procedure beginning with a rigid cylindrical tank with beams and without liquid, followed by treating the sloshing characteristics in a rigid cylindrical tank.

In the numerical calculations, the unknown parameters A_{1s} and B_v in Eq. (45) included 10 terms for each parameter to satisfy the requirements for engineering data. The liquid height parameter was $h_0 = h / R = 1.0$ and, as mentioned above, the positions of the roots of the two beams e from the tank bottom were taken as equal to that of the center of gravity *G*, i.e., $\bar{e} = e / R = h_0 / 2$.

4.1. Vibration characteristics of "rigid cylindrical tank–two beams" system

First, the vibration characteristics of a "rigid cylindrical tank–two beams" system are considered, which corresponds to a scenario in which the spacecraft runs out of fuel. In this case, the liquid displacement vector A_{1s} is omitted from Eq. (45).

4.1.1. Influence of inertia moment of tank $\bar{J}_t$

Variations of the natural circular frequency Ω with inertia moment $\bar{J}_t$ up to the third mode are shown in Fig. 2(a), when $\lambda = 10, 100$. In the figure, results for $\lambda = 10$ are shown as dashed lines, while those for $\lambda = 100$ are shown as solid lines. In Fig. 2(b) and 2(c), vibration modes when $\bar{J}_t = 10^{-2}$, $\bar{J}_t = 10^{2}$ are presented.

Here, we shall consider the frequency equation when the moment of inertia $\bar{J}_t$ tends toward zero or ∞. In these cases, Eq. (37) renders:

$$\begin{aligned} &\frac{2\lambda^2}{\bar{J}_t}\left(\cosh\alpha_u \sin\alpha_u - \sinh\alpha_u \cos\alpha_u\right) + \frac{2\alpha_u^2}{\bar{J}_t}\left(\cosh\alpha_u \sin\alpha_u + \sinh\alpha_u \cos\alpha_u\right) \\ &+ \frac{4\alpha_u\lambda}{\bar{J}_t}\sinh\alpha_u \sin\alpha_u + \lambda^2\alpha_u^3 \cosh\alpha_u \cos\alpha_u + \lambda^2\alpha_u^3 = 0 \end{aligned} \tag{47}$$

or

$$\begin{aligned} &2\left(\cosh\alpha_u \sin\alpha_u - \sinh\alpha_u \cos\alpha_u\right) + \frac{2\alpha_u^2}{\lambda^2}\left(\cosh\alpha_u \sin\alpha_u + \sinh\alpha_u \cos\alpha_u\right) \\ &+ \frac{4\alpha_u}{\lambda}\sinh\alpha_u \sin\alpha_u + \bar{J}_t\alpha_u^3 \cosh\alpha_u \cos\alpha_u + \bar{J}_t\alpha_u^3 = 0 \end{aligned} \tag{48}$$

First, when $\bar{J}_t \to \infty \left(\bar{m}_t \to \infty\right)$, Eq. (47) renders:

$$\cosh\alpha_u \cos\alpha_u + 1 = 0 \tag{49}$$

which is the frequency equation for a clamped–free beam.

Next, when $\bar{J}_t \to 0$ $(\bar{m}_t \to 0)$, Eq. (48) renders:

$$2\left(\cosh\alpha_u \sin\alpha_u - \sinh\alpha_u \cos\alpha_u\right) + \frac{2\alpha_u^2}{\lambda^2}\left(\cosh\alpha_u \sin\alpha_u + \sinh\alpha_u \cos\alpha_u\right) + \frac{4\alpha_u}{\lambda}\sinh\alpha_u \sin\alpha_u = 0 \tag{50}$$

In addition, letting $\lambda \to \infty$, we obtain:

$$\tan\alpha_u - \tanh\alpha_u = 0 \tag{51}$$

This is the natural frequency equation for a simply supported–free beam.

For a free–free beam with length $2l$ we obtain:

$$\cosh 2\alpha_u \cos 2\alpha_u - 1 = 0 \tag{52}$$

One finds from Fig. 2(a) that, as $\bar{J}_t$ increases, coupled natural circular frequencies Ω decrease. When $\bar{J}_t \to \infty$ $(\bar{m}_t \to \infty)$, as anticipated from Eq. (49), coupled natural frequencies tend toward those of the beam with a clamped–free boundary condition, i.e., blue circles in the figure as Ω = 3.52, 22.03, 61.70, and there seems to be no rotational motion of the main body of the satellite, as shown in Fig. 2(c), because the moment of inertia of the tank is large. In Fig. 2(c), maximum amplitude of the beam is normalized as unity.

When $\bar{J}_t \to 0$ $(\bar{m}_t \to 0)$, coupled natural circular frequencies tend toward those of a free–free beam with length $2l$ of the even–order modes, which are shown in Fig. 2(a) with red circles as Ω = 15.42, 49.97, 104.25; when $\lambda = 100$, or those of a simply supported–free beam, they are shown with green Δ as Ω = 15.42, 49.97, 104.25. In addition, the influence of aspect ratio λ on the natural frequency is significant for a smaller $\bar{J}_t$, as shown in Fig. 2(b), and with an increase in the inertia moment, rotatory motion of the main body becomes large.

4.1.2. Variation of vibration modes

We next examine the influence of the moment of inertia of the rigid tank $\bar{J}_t$ on the vibration modes of the system, as shown in Fig. 3, in which two beams behave with antisymmetric motion. In the figure, red dash-dotted lines are the first mode, blue solid lines are the second mode, and black dashed lines are the third mode.

In the odd order vibration modes, the roots of beams rotate in the clockwise direction, while in the even order vibration modes they rotate in the counterclockwise direction, and the rotation amplitude becomes large for lower vibration mode. Comparing Fig. 4(a) to(c), one can find that the rotation angle becomes gradually small with an increase in $\bar{J}_t$.

4.1.3. Influence of aspect ratio λ

Next, variations of the natural circular frequencies Ω with aspect ratio $\lambda = l/R$ are shown in Fig. 4 when $\bar{J}_t = 10^{-4}, 10^{-2}$. In the figure, natural circular frequencies of a simply supported–free beam are presented with green triangles Δ as Ω = 15.42, 49.97, 104.25, while those of a free–free beam with length $2l$ of the even order modes are presented with red circles $\bigcirc$ as Ω = 15.42, 49.97, 104.25.

In addition, in Fig. 4(b) and 4(c), vibration modes when $\lambda = 1$ and 100 are presented. When λ is large, natural circular frequencies tend toward those of a simply supported–free beam or of a free–free beam with length $2l$ of the even order modes when $\bar{J}_t = 10^{-4}$, and the displacement of the beam becomes more significant than that of rotation of the tank, as shown in Fig. 4(c). Contrary to this, when λ is small, rotation of the tank becomes large. Influence of the moment of inertia $\bar{J}_t$ on the natural frequency becomes significant for larger aspect ratio λ.

4.2. Sloshing in a rigid tank without beams

Next, we consider liquid in a rigid cylindrical tank in space, neglecting two beams as appendages. In this case, the beam displacement B_v is omitted in Eq. (45).

In the present study, as we consider the pitching vibration of the space model, the vibration mode of the liquid in the tank is that with the nodal diameter $N = 1$. Hereafter, we express the number of nodal circle as m.

4.2.1. Variation of natural circular frequency with contact angle θ_0

Variations of the natural circular frequencies up to the third mode with contact angle θ_0 are shown in Fig. 5. In the figure, solid lines are the results of the present study with N = 1 mode, while dashed lines are those of the former study of the axisymmetric mode with N = 0 (see Chiba et al. [23]). In the present results with N = 1 mode, natural circular frequencies of the second and third mode are maximum at $\theta_0 = 90^\circ$ except the first mode, while in the N = 0 mode natural frequencies are higher than those of the N = 1 mode and are maximum at $\theta_0 = 90^\circ$, independent of the vibration order.

4.2.2. Variation of vibration mode

The liquid's free surface axis symmetrically deforms as meniscus due to surface tension, and a small amplitude vibration occurs around it (see Chiba et.al. [23]). Variations of the vibration mode with contact angle

θ_0 are shown in Fig. 6. In the figure, the black dotted line is the result when $\theta_0 = 70^\circ$, the blue solid line is that when $\theta_0 = 90^\circ$, and the red dash-dotted line is that when $\theta_0 = 110^\circ$. One can see the nodal diameter at $\rho = 0$. Additionally, the influence of the contact angle θ_0 can be seen in the neighborhood of the tank wall.

4.3. Coupled system

Finally, we proceed to the coupled case when a liquid is in the tank. In this section, the results when $\theta_0 = 70^\circ$ are presented as a representative case.

First, we consider the influence of the moment of inertia of the tank $\bar{J}_t$ on the natural frequency and vibration mode. Variations of coupled natural frequencies up to the fourth mode with $\bar{J}_t$ are shown in Fig. 7(a). In the figure, the dashed pink line represents the frequency curve in which displacement of beams is predominant, while the other curves are those in which liquid motion is predominant. The former curve corresponds to that of the tank–beam system without liquid, as presented in Fig. 3. In addition, the crossing region between frequency curves of the 3rd and 4th modes is enlarged in Fig. 7(b).

As shown in Fig. 7(a), the frequency curve with the dashed pink line, in which beam displacement is predominant, decreases as $\bar{J}_t$ increases, while that in which liquid motion is predominant does not change with $\bar{J}_t$. Strong coupling between bending motion of the beams and liquid sloshing motions in the tank is expected in the crossing region of the frequency curves, as shown in Fig. 7(b). The vibration modes with the higher frequency of the two frequency curves, when $\bar{J}_t = 0.03, 1.0$, are shown in Fig. 8. In Fig. 8(a) bending motion of the beam and pitching motion of the tank are predominant and a small amount of sloshing can be seen, while in Fig. 9(b) sloshing motion is predominant and there seems to be no coupling with beam motion. Vibration mode exchange is recognized before and after the crossing.

5. Conclusions

This study involved the analysis of the influence of liquid sloshing on the pitching dynamics of flexible space structures with on-board liquid in zero-gravity conditions. The main body of the spacecraft was modeled as a rigid tank, flexible appendages as two elastic beams, and on-board liquid as an ideal liquid. The obtained results are summarized as follows:

i) *Coupled system without liquid*

- When the moment of inertia of the tank $\overline{J}_t$ was large, the main body did not show any motion, and the natural frequency of the system tended to correspond to that of a clamped–free beam; simultaneously, the rotation angle of the root of the beam became small.
- While the moment of inertia of the tank $\overline{J}_t$ was small, the natural frequency tended toward that of a free–free beam with length $2l$, of the even order mode, or that of a simply supported–free beam, in which the vibration mode's (as the main body was located at the middle of the free–free beam) rotation amplitude at the root increased.
- Influence of the aspect ratio on the natural frequency was larger for a smaller $\overline{J}_t$.

ii) *Sloshing characteristics in a tank floating in space*

- Natural frequencies with $N = 1$ were lower than those with $N = 0$ (Chiba et al., 2017).
- Concerning the variations of the natural frequencies with contact angle θ_0, natural frequencies of the second and third mode took maximum at $\theta_0 = 90^\circ$ except the first mode, while in the $N = 0$ mode they were maximum at $\theta_0 = 90^\circ$, independent of the vibration order.

iii) *Coupled system*

- Depending on the magnitude of the inertia moment of the system, i.e., the sum of that of tank and that of liquid in the tank, coupled vibration occurred at the crossing region of two frequency curves in which liquid motion or beam motion were predominant.
- During the operation of satellites, decreases in fuel may lead to the crossing of two natural frequency curves, that would introduce strong coupling of the two motions, i.e., liquid sloshing and beam vibration.

References

[1] H.N. Abramson, The dynamic behavior of liquids in moving containers, chapter 11, NASA SP-106 (1966).

[2] H.F. Bauer, W. Eidel, Linear liquid oscillations in cylindrical container under zero gravity, Appl. Microgravity Tech **2** (1990a) 212-220.

[3] H.F. Bauer, W. Eidel, Small amplitude liquid oscillations in a rectangular container under zero gravity, Zeitsschrift fur Flugwissenschaften und Weltraumforschung **14** (1990b) 1-8.

[4] B.N. Agrawal, Dynamic characteristics of liquid motion in partially filled tanks of a spinning spacecraft, J. Guid. Contr. Dyn. **16**(4) (1993) 636-640.

[5] K. Komatsu, Modeling of the dynamic behavior of liquids in spacecraft, Int. J. Microgravity Science and Application **16**(3) (1999) 182-190.

[6] M. Chiba, H. Watanabe, H.F. Bauer, Hydroelastic coupled vibrations in a cylindrical container with a membrane bottom, containing liquid with surface tension, J. Sound Vibr. **251**(4) (2002) 717-740.

[7] M. Utsumi, A mechanical model for low-gravity sloshing in an axisymmetric tank, Trans. ASME, J. Applied Mechanics **71** (2004) 724-730.

[8] H. Yuanjun, M. Xingrui, W. Pigping, W. Benli, Low-gravity liquid nonlinear sloshing analysis in a tank under pitching excitation, J. Sound Vibr. **299** (2007) 164-177.

[9] M.D. Berglund, C.E. Bassett, J.M. Kelso, J. Mishic, D. Schrange, The Boeing Delta IV launch vehicle–Pulse-settling approach for second-stage hydrogen propellant management, Acta Astronautica **61** (2007) 416-424.

[10] D-L. Cui, S-Z. Yan, X-S. Guo, R. X. Gao, Parametric resonance of liquid sloshing in partially filled spacecrafts during the powered-flight phase of rocket, Aer. Sci. Tech., **35** (2014) 93-105.

[11] M.A. Noorian, H. Haddadpour, M. Ebrahimian, Stability analysis of elastic launch vehicles with fuel sloshing in planar flight using a BEM-FEM model, Aero. Sci. Tech., 53 (2016) 74-84.

[12] J.P.B. Vreeburg, Sloshsat spacecraft calibration at stationary spin rates, J. Space. Rockets **45**(1) (2008) 65-75.

[13] M. Lazzarin, M. Biolo, A. Bettella, M. Manente, R.D. Forno, D. Pavarin, EUCLID satellite: Sloshing model development through computational fluid dynamics, Aero. Sci. Tech., **36** (2014) 44-54.

[14] J.E. McIntyre, J.M. McIntyre, Some effects of propellant motion on the performance of spinning satellites, Acta Astronaut. **9**(12) (1982) 645-661.

[15] P. Santini, R. Barboni, Motion of orbiting spacecrafts with a sloshing fluid, Acta Astronaut. **5**(7-8) (1978) 467-490.

[16] P. Santini, R. Barboni, A minicomputer finite elements program for microgravity hydroelastic analysis, Acta Astronaut. **10**(2) (1983) 81-90.

[17] J. Lü, J. Li, T. Wang, Dynamic response of liquid-filled rectangular tank with elastic appendages under pitching excitation, Appl. Math. Mech. **28**(3) (2007) 351-359.

[18] C. Farhat, E.K. Chiu, D. Amsallem, Modeling of fuel sloshing and its physical effects on

flutter, AIAA J. **51**(9) (2013) 2252-2265.
[19] P. Gasbarri, M. Sabatini, A. Pisculli, Dynamic modelling and stability parametric analysis of a flexible spacecraft with fuel slosh, Acta Astronaut. (2016) **127** 141-159.
[20] Y. Baozeng, W. Wenjun, Y. Yulong, Modelling and coupling dynamics of the spacecraft with multiple propellant tanks, AIAA J. **54**(11) (2016) 3608-3618.
[21] Z. Zhou, H. Huang, Constraint surface model for large amplitude sloshing of the spacecraft with multiple tanks", Acta Astronaut., **111** (2015) 222-229.
[22] M. Chiba, S. Chiba, K. Takemura, Coupled hydroelastic vibrations of a liquid on flexible space structures under zero-gravity– part I. mechanical model, Coupled Syst. Mech. **2**(4) (2013) 303-327.
[23] M. Chiba, H. Magata, Influence of liquid sloshing on dynamics of flexible space structures, J. Sound Vibr., **401** (2017)1-22.
[24] M. Chiba, H. Magata, Influence of torsional rigidity of flexible appendages on the dynamics of flexible spacecrafts, Coupled Syst. Mech. **8**(1) (2019) 19-38.
[25] K. Kimura, H. Takahara, T. Ito, M. Sakata, Nonlinear liquid oscillation in a circular cylindrical tank subjected to pitching excitation (in Japanese), Trans. JSME C **58**(556) (1992) 110-117.
[26] J.C. Luke, A variational principle for a fluid with a free surface, J. Fluid Mech. **27**(2) (1967) 395-397.
[27] K. Komatsu, Sloshing (in Japanese), p. 112 (2015) Morikita Publishing.
[28] H.F. Bauer, Fluid oscillations in the containers of a space vehicle and their influence upon stability, (1964) NASA TR R-187.

[xx] H. Takahara, K. Kimura, Frequency response of sloshing in an annular cylindrical tank subjected to pitching excitation, J. Sound and Vibr., **331** (2012) 3199-3212.
[vv] Y. BaoZeng, Large-scale amplitude liquid sloshing in container under pitching excitation, Chinese Science Bulletin **53** (2008) 3816-3823.
[bb] H. N. Abramson, Liquid sloshing in rigid cylindrical tanks under-going pitching motion, (1961) Tech. Rept. 11, SwRI.

Appendix A. Force and moment relation between rigid tank and elastic beams

Force and moment balances between the rigid tank and the elastic beam of the right-hand side with No. 1 are shown in Fig. A1. In the figure, reaction force and reaction moment are represented as R_i and M_i, $i = 1, 2$, respectively. Two elastic beams each exhibit asymmetric motion each; only the right-hand side beam with $i = 1$ is presented.

Appendix B Derivation of Eigenfunction Eq. (38)

Eigenfunction of the elastic beams which satisfies the non-dimensional equations of motion Eq. (11)" is assumed as:

$$\tilde{w}_{iu}\left(\xi_i\right) = C_1 \cosh \alpha_u \xi_i + C_2 \cos \alpha_u \xi_i + C_3 \sinh \alpha_u \xi_i + C_4 \sin \alpha_u \xi_i \qquad \text{(B-1)}$$

where $i = 1, 2,$ $C_1 \sim C_4$ are unknown constants, and parameters α_u satisfy frequency equation (37).

$$\alpha_u^2 = \Omega \qquad \text{(B-2)}$$

Substituting Eq. (B-1) into the boundary conditions Eq. (12)" to Eq. (17)",

at $\xi_i = 0$:

$$C_1 + C_2 = \frac{1}{\lambda}\bar{\theta} \qquad (12)'''$$

$$C_3 \alpha_u + C_4 \alpha_u = \bar{\theta} \qquad (13)'''$$

$$C_1 {\alpha_u}^2 - C_2 {\alpha_u}^2 = \tilde{M}_i \qquad (14)'''$$

$$-C_3 \alpha_u^3 + C_4 \alpha_u^3 = \tilde{R}_i \qquad (15)'''$$

at $\xi_i = 1$:

$$C_1 \alpha_u^2 \cosh \alpha_u - C_2 \alpha_u^2 \cos \alpha_u + C_3 \alpha_u^2 \sinh \alpha_u - C_4 \alpha_u^2 \sin \alpha_u = 0 \qquad (16)'''$$

$$-C_1 \alpha_u^3 \sinh \alpha_u - C_2 \alpha_u^3 \sin \alpha_u - C_3 \alpha_u^3 \cosh \alpha_u + C_4 \alpha_u^3 \sin \alpha_u = 0 \qquad (17)'''$$

Eliminating $\bar{\theta}$ from Eq. (12)" and Eq. (13)", one obtains:

$$\lambda C_1 + \lambda C_2 - C_3 \alpha_u - C_4 \alpha_u = 0 \qquad \text{(B-3)}$$

Then substituting Eq. (B-2), Eq. (12)"', Eq. (14)", and Eq. (15)"', into Eq. (10)" one obtains Eq. (B-4):

$$\bar{J}_t \Omega^2 \bar{\theta} + 2\left(\tilde{M}_i + \frac{1}{\lambda}\tilde{R}_i \right) = 0 \qquad (10)''$$

$$\bar{J}_t\alpha_u^4\left(\lambda^2 C_1+\lambda^2 C_2\right)+2\left(C_1\lambda\alpha_u^2-C_2\lambda\alpha_u^2-C_3\alpha_u^3+C_4\alpha_u^3\right)=0 \tag{B-4}$$

Rearranging Eq. (16)"', Eq. (17)", Eq. (B-3), Eq. (B-4) into a matrix form,

$$\begin{pmatrix} \cosh\alpha_u & -\cos\alpha_u & \sinh\alpha_u & -\sin\alpha_u \\ \sinh\alpha_u & \sin\alpha_u & \cosh\alpha_u & -\cos\alpha_u \\ \lambda & \lambda & -\alpha_u & -\alpha_u \\ \bar{J}_t\alpha_u^2\lambda^2+2\lambda & \bar{J}_t\alpha_u^2\lambda^2-2\lambda & -2\alpha_u & 2\alpha_u \end{pmatrix}\begin{Bmatrix} C_1 \\ C_2 \\ C_3 \\ C_4 \end{Bmatrix}=0 \tag{B-5}$$

As the condition to obtain non-trivial solutions C_1 to C_4,

$$\begin{vmatrix} \cosh\alpha_u & -\cos\alpha_u & \sinh\alpha_u & -\sin\alpha_u \\ \sinh\alpha_u & \sin\alpha_u & \cosh\alpha_u & -\cos\alpha_u \\ \lambda & \lambda & -\alpha_u & -\alpha_u \\ \bar{J}_t\alpha_u^2\lambda^2+2\lambda & \bar{J}_t\alpha_u^2\lambda^2-2\lambda & -2\alpha_u & 2\alpha_u \end{vmatrix}=0 \tag{B-6}$$

one obtains frequency equation (37):

$$\begin{aligned} &2\lambda^2\left(\cosh\alpha_u\sin\alpha_u-\sinh\alpha_u\cos\alpha_u\right)+2\alpha_u^2\left(\cosh\alpha_u\sin\alpha_u+\sinh\alpha_u\cos\alpha_u\right) \\ &+4\lambda\alpha_u\sinh\alpha_u\sin\alpha_u+\bar{J}_t\lambda^2\alpha_u^3\cosh\alpha_u\cos\alpha_u+\bar{J}_t\lambda^2\alpha_u^3=0 \end{aligned} \tag{37}$$

Finally, one obtains the eigenfunction from $C_1 \sim C_4$ relations, as:

$$\begin{aligned} \tilde{w}_{iu}\left(\xi_i\right)=&\left\{\lambda\sin\alpha_u\cosh\alpha_u-\lambda\cos\alpha_u\sinh\alpha_u+\alpha_u+\alpha_u\cos\alpha_u\cosh\alpha_u+\alpha_u\sin\alpha_u\sinh\alpha_u\right\}\cosh\alpha_u\xi_i \\ &+\left\{-\lambda\sin\alpha_u\cosh\alpha_u+\lambda\cos\alpha_u\sinh\alpha_u+\alpha_u+\alpha_u\cos\alpha_u\cosh\alpha_u-\alpha_u\sin\alpha_u\sinh\alpha_u\right\}\cos\alpha_u\xi_i \\ &+\left\{\lambda\cos\alpha_u\cosh\alpha_u-\lambda\sin\alpha_u\sinh\alpha_u+\lambda-\alpha_u\cos\alpha_u\sinh\alpha_u-\alpha_u\sin\alpha_u\cosh\alpha_u\right\}\sinh\alpha_u\xi_i \\ &+\left\{\lambda\cos\alpha_u\cosh\alpha_u+\lambda\sin\alpha_u\sinh\alpha_u+\lambda+\alpha_u\cos\alpha_u\sinh\alpha_u+\alpha_u\sin\alpha_u\cosh\alpha_u\right\}\sin\alpha_u\xi_i \end{aligned} \tag{36}$$

Appendix C Moment of inertia of liquid in a cylindrical tank $\bar{J}_f$

We shall derive the moment of inertia of liquid in a cylindrical tank under the assumption that the liquid free-surface does not vibrate, maintaining the meniscus shape with surface tension.

Assuming a pitching angle of $\theta(\tau)$ and a liquid potential of $\phi\left(\rho,\varphi,\eta,\tau\right)$ in the form of Eq. (C-1), and a velocity potential that satisfies Laplace equation (1)' and the boundary conditions at the side wall and the bottom of the tank, Eq. (C-2) and Eq. (C-3), is assumed to be in the form as Eq. (C-4).

$$\begin{aligned} \theta\left(\tau\right)&=\bar{\theta}\cos\Omega\tau \\ \phi\left(\rho,\varphi,\eta,\tau\right)&=-\Omega\bar{\phi}\left(\rho,\varphi,\eta\right)\sin\Omega\tau \end{aligned} \tag{C-1}$$

At the side wall:

$$\left.\frac{\partial\bar{\phi}\left(\rho,\varphi,\eta\right)}{\partial\rho}\right|_{\rho=1}=-\bar{\theta}\eta\cos\varphi \tag{C-2}$$

At the bottom:

$$\left.\frac{\partial \bar{\phi}\left(\rho,\varphi,\eta\right)}{\partial \eta}\right|_{\eta=-\bar{e}} = \bar{\theta}\rho\cos\varphi \tag{C-3}$$

$$\bar{\phi}\left(\rho,\varphi,\eta\right) = 4\bar{\theta}\cos\varphi\sum_i \frac{J_1\left(\varepsilon_{1i}\rho\right)\sinh\left(\varepsilon_{1i}\eta\right)}{\varepsilon_{1i}\left(\varepsilon_{1i}{}^2-1\right)J_1\left(\varepsilon_{1i}\right)\cosh\left(\varepsilon_{1i}\bar{e}\right)} - \bar{\theta}\rho\eta\cos\varphi \tag{C-4}$$

Moment of inertia about an axis which passes through the center of gravity and is parallel to the liquid surface is given by Komatsu (2015)as:

$$J_f = \frac{\rho_f}{\dot{\theta}^2}\int_V\left(\frac{\partial\Phi}{\partial n}\right)^2 dV = \frac{\rho_f}{\dot{\theta}^2}\int_S \Phi\frac{\partial\Phi}{\partial n}dS \tag{C-5}$$

In the non-dimensional form,

$$\bar{J}_f = \frac{1}{\pi}\frac{1}{\left(\frac{d\theta}{d\tau}\right)^2}\int_{\bar{V}}\left(\frac{\partial\phi}{\partial\bar{n}}\right)^2 d\bar{V} = \frac{1}{\pi}\frac{1}{\left(\frac{d\theta}{d\tau}\right)^2}\int_{\bar{S}}\phi\frac{\partial\phi}{\partial\bar{n}}d\bar{S} \tag{C-5}'$$

Substituting Eq. (C-1) into the above equation:

$$\bar{J}_f = \frac{1}{\pi}\frac{1}{\bar{\theta}^2}\int_{\bar{V}}\left(\frac{\partial\bar{\phi}}{\partial\bar{n}}\right)^2 d\bar{V} = \frac{1}{\pi}\frac{1}{\bar{\theta}^2}\int_{\bar{S}}\bar{\phi}\frac{\partial\bar{\phi}}{\partial\bar{n}}d\bar{S} \tag{C-5}''$$

Here for convenience, we assume Eq. (C-4) is in the form of:

$$\bar{\phi}\left(\rho,\varphi,\eta\right) = -\bar{\theta}\bar{x}\eta + \bar{\theta}\,\Pi\left(\rho,\varphi,\eta\right) \tag{C-4}'$$

and by substituting this equation into Eq. (C-5)'' and rearranging it as:

$$\begin{aligned}
\bar{J}_f &= \bar{J}_1 + \bar{J}_2 + \bar{J}_3 \\
\bar{J}_1 &= \frac{1}{\pi}\int_{\bar{V}}\left\{\bar{x}^2+\eta^2\right\}d\bar{V} \\
\bar{J}_2 &= \frac{1}{\pi}\int_{\bar{V}}\left\{\left(\frac{\partial\Pi}{\partial\bar{x}}\right)^2+\left(\frac{\partial\Pi}{\partial\bar{y}}\right)^2+\left(\frac{\partial\Pi}{\partial\eta}\right)^2\right\}d\bar{V} \\
\bar{J}_3 &= -\frac{2}{\pi}\int_{\bar{V}}\left\{\eta\frac{\partial\Pi}{\partial\bar{x}}+\bar{x}\frac{\partial\Pi}{\partial\eta}\right\}d\bar{V}
\end{aligned} \tag{C-6}$$

In the above, $\bar{J}_1$ is subdivided into two cases depending on the contact angle $\theta_0 \le 90^\circ$ and $90^\circ < \theta_0$, see Fig. A2.

$$\theta_0 \le 90^\circ \qquad \begin{aligned} \bar{J}_1 &= \frac{1}{\pi}\int_0^1 d\rho \int_0^{2\pi} d\varphi \int_{-\bar{e}}^{h_0-\bar{e}+\eta_0(0)} \left(\rho^2\cos^2\varphi+\eta^2\right)\rho d\eta \\ &+ \frac{1}{\pi}\int_0^1 d\rho \int_0^{2\pi} d\varphi \int_{h_0-\bar{e}+\eta_0(0)}^{h_0-\bar{e}+\eta_0(1)} \left(\rho^2\cos^2\varphi+\bar{\eta}_{01}{}^2(\rho)\right)\rho d\eta \end{aligned} \qquad \text{(C-7(a))}$$

$$90^\circ < \theta_0 \qquad \begin{aligned} \bar{J}_1 &= \frac{1}{\pi}\int_0^1 d\rho \int_0^{2\pi} d\varphi \int_{-\bar{e}}^{h_0-\bar{e}+\eta_0(1)} \left(\rho^2\cos^2\varphi+\eta^2\right)\rho d\eta \\ &+ \frac{1}{\pi}\int_0^1 d\rho \int_0^{2\pi} d\varphi \int_{h_0-\bar{e}+\eta_0(1)}^{h_0-\bar{e}+\eta_0(0)} \left(\rho^2\cos^2\varphi+\bar{\eta}_{02}{}^2(\rho)\right)\rho d\eta \end{aligned} \qquad \text{(C-7(b))}$$

where

$$\eta_0(\rho) = \frac{2\left(1-\sin^3\theta_0\right)}{3\cos^3\theta_0} - \frac{1}{\cos\theta_0}\sqrt{1-\left(\rho\cos\theta_0\right)^2} \qquad \text{(C-8)}$$

$$\bar{\eta}_{01}(\rho) = \frac{2\left(1-\sin^3\theta_0\right)}{3\cos^3\theta_0} - \frac{1}{\cos\theta_0}\sqrt{1-\left(\rho\cos\theta_0\right)^2} - \eta_0(0) = \frac{1}{\cos\theta_0}\left\{1-\sqrt{1-\left(\rho\cos\theta_0\right)^2}\right\} \qquad \text{(C-9)}$$

$$\bar{\eta}_{02}(\rho) = \frac{2\left(1-\sin^3\theta_0\right)}{3\cos^3\theta_0} - \frac{1}{\cos\theta_0}\sqrt{1-\left(\rho\cos\theta_0\right)^2} - \eta_0(1) = \frac{\sqrt{1-\left(\cos\theta_0\right)^2}-\sqrt{1-\left(\rho\cos\theta_0\right)^2}}{\cos\theta_0} \qquad \text{(C-10)}$$

As the results, we obtain:

$$\begin{aligned} \bar{J}_f &= \bar{J}_1 + \bar{J}_2 + \bar{J}_3 \\ \bar{J}_1 &= \frac{1}{4}A_1 + \frac{1}{3}\left\{A_1{}^3 - 3A_1{}^2\bar{e} + 3A_1\bar{e}^2\right\} + \left\{\eta_0(1)-\eta_0(0)\right\}\int_0^1\left\{\frac{2}{3}\rho\bar{\eta}_{01}{}^2(\rho)+\rho^3\right\}d\rho \qquad \left(\theta_0 \le 90^\circ\right) \\ \bar{J}_1 &= \frac{1}{4}A_2 + \frac{1}{3}\left\{A_2{}^3 - 3A_2{}^2\bar{e} + 3A_2\bar{e}^2\right\} + \left\{\eta_0(0)-\eta_0(1)\right\}\int_0^1\left\{\frac{2}{3}\rho\bar{\eta}_{02}{}^2(\rho)+\rho^3\right\}d\rho \qquad \left(90^\circ < \theta_0\right) \\ \bar{J}_2 &= 8\sum_i \frac{1}{\varepsilon_{1i}^3\left(\varepsilon_{1i}^2-1\right)}\tanh\left(\varepsilon_{1i}\bar{e}\right) \\ &+ 16\sum_i\sum_k \frac{\int_0^1 J_1(\varepsilon_{1i}\rho)J_1(\varepsilon_{1k}\rho)\sinh\left[\varepsilon_{1i}\left\{h_0-\bar{e}+\eta_0(\rho)\right\}\right]\cosh\left[\varepsilon_{1k}\left\{h_0-\bar{e}+\eta_0(\rho)\right\}\right]\rho\sqrt{1+\left\{\frac{\partial\eta_0(\rho)}{\partial\rho}\right\}^2}\,d\rho}{\varepsilon_{1i}\left(\varepsilon_{1i}^2-1\right)\left(\varepsilon_{1k}^2-1\right)J_1(\varepsilon_{1i})J_1(\varepsilon_{1k})\cosh\left(\varepsilon_{1i}\bar{e}\right)\cosh\left(\varepsilon_{1k}\bar{e}\right)} \\ \bar{J}_3 &= -\bar{e} - 8\int_0^1\left\{h_0-\bar{e}+\eta_0(\rho)\right\}\sum_i \frac{J_1(\varepsilon_{1i}\rho)\cosh\left[\varepsilon_{1i}\left\{h_0-\bar{e}+\eta_0(\rho)\right\}\right]}{\left(\varepsilon_{1i}^2-1\right)J_1(\varepsilon_{1i})\cosh\left(\varepsilon_{1i}h_0\right)}\rho^2\sqrt{1+\left\{\frac{\partial\eta_0(\rho)}{\partial\rho}\right\}^2}\,d\rho \end{aligned} \qquad \text{(C-11)}$$

Here, putting contact angle $\theta_0 = 90^\circ$ and $\bar{e} = h_0/2$, we obtain:

$$
\begin{aligned}
\bar{J}_f &= \bar{J}_1 + \bar{J}_2 + \bar{J}_3 \\
\bar{J}_1 &= \frac{1}{4} h_0 + \frac{{h_0}^3}{12} \\
\bar{J}_2 &= 16 \sum_i \frac{1}{\varepsilon_{1i}^3 \left(\varepsilon_{1i}^2 - 1 \right)} \tanh\left(\varepsilon_{1i} \frac{h_0}{2} \right) \\
\bar{J}_3 &= -h_0
\end{aligned}
\tag{C-12}
$$

$$
\begin{aligned}
\bar{J}_f &= \frac{1}{4} h_0 + \frac{{h_0}^3}{12} + 16 \sum_i \frac{1}{\varepsilon_{1i}^3 \left(\varepsilon_{1i}^2 - 1 \right)} \tanh\left(\varepsilon_{1i} \frac{h_0}{2} \right) - h_0 \\
&= \frac{1}{4} h_0 + \frac{{h_0}^3}{12} - 8 h_0 \sum_i \frac{1 - 2 / \varepsilon_{1i} h_0}{\varepsilon_{1i}^3 \left(\varepsilon_{1i}^2 - 1 \right)} \tanh\left(\varepsilon_{1i} \frac{h_0}{2} \right)
\end{aligned}
\tag{C-13}
$$

Here, we used the following relation, see Komatsu [27]:

$$
\sum_i \frac{1}{\varepsilon_{1i}^2 \left(\varepsilon_{1i}^2 - 1 \right)} = \frac{1}{8}
\tag{C-14}
$$

Expressing Eq. (C-13) in a dimensional form, we obtain the moment of inertia that is consistent with the results of Bauer [28] and Komatsu [27]:

$$
J_f = m_f \left(\frac{R^2}{4} + \frac{h^2}{12} \right) - 8 m_f R^2 \sum_i \frac{1 - 2R / \varepsilon_{1i} h}{\varepsilon_{1i}^2 \left(\varepsilon_{1i}^2 - 1 \right)} \tanh\left(\frac{\varepsilon_{1i} h}{2R} \right)
\tag{C-15}
$$

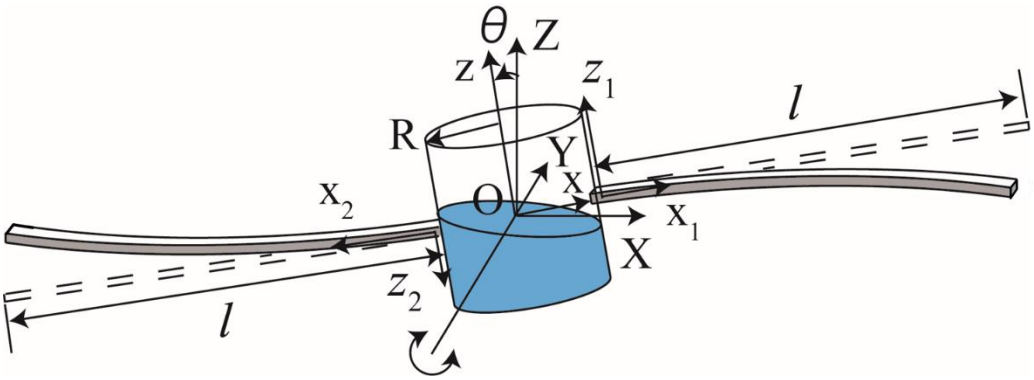

(a) Spacecraft with two appendages.

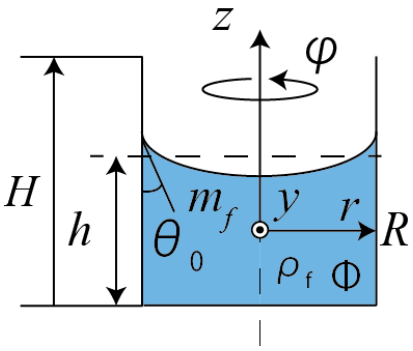

(b) Cylindrical tank.

Fig. 1. Flexible spacecraft model with liquid tank; (a) Spacecraft with two appendages.; (b) Cylindrical tank.

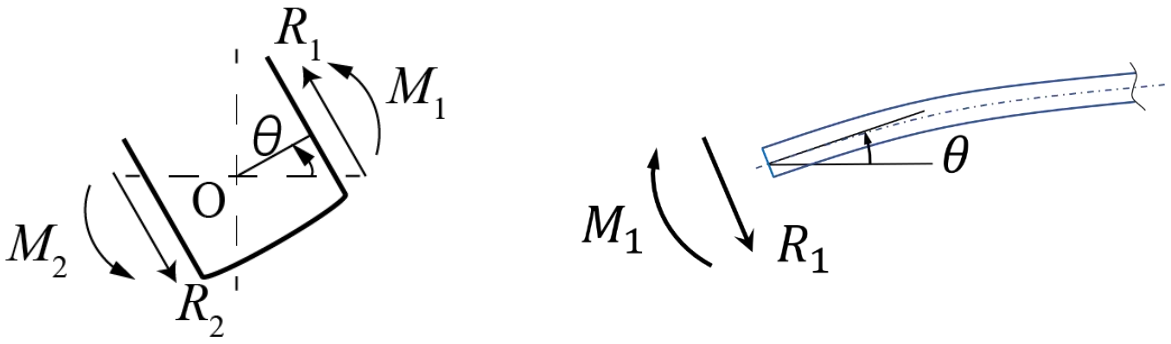

(a) Rigid cylindrical tank. (b) Elastic beam No. 1.

Fig. 2. Force and moment diagram for rigid cylindrical tank and elastic beam 1.; (a) Rigid cylindrical tank.; (b) Elastic beam No. 1.

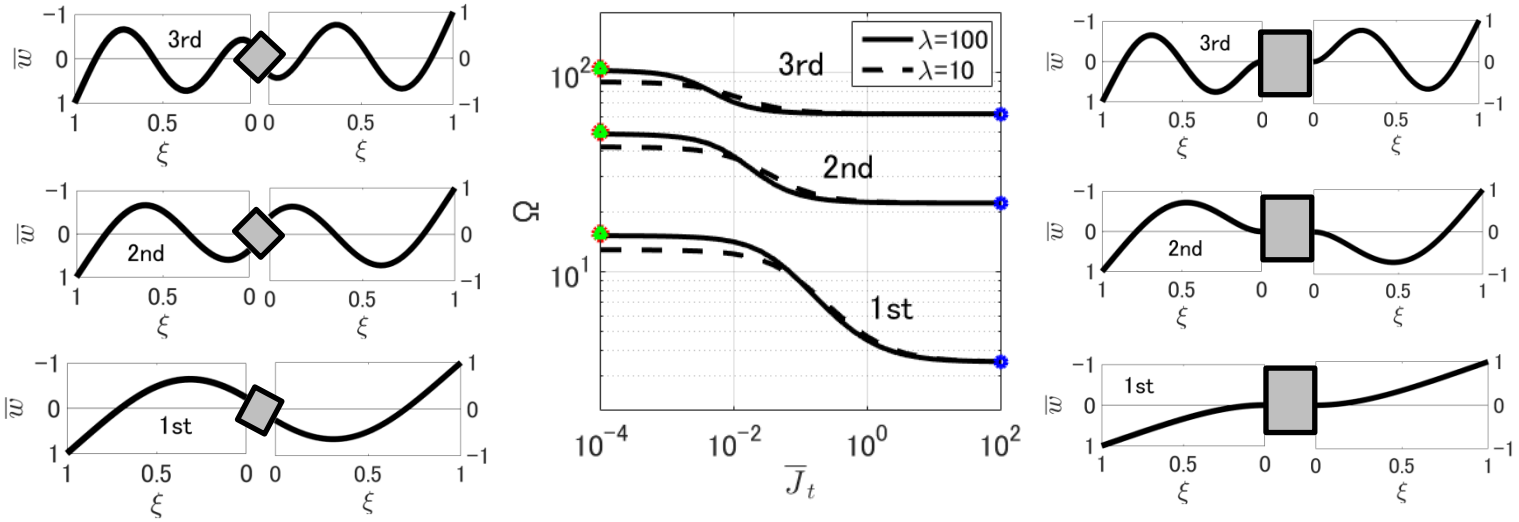

(b) $\bar{J}_t = 10^{-2}$.　　(a) Natural frequency with $\bar{J}_t$.　　(c) $\bar{J}_t = 10^{2}$.

Fig. 3. Variations of natural frequency Ω and vibration mode with inertia moment $\bar{J}_t$, $\lambda = 10,\ 100$.; (a) Natural frequency. ; (b) $\bar{J}_t = 10^{-2}$.; (c) $\bar{J}_t = 10^{2}$.

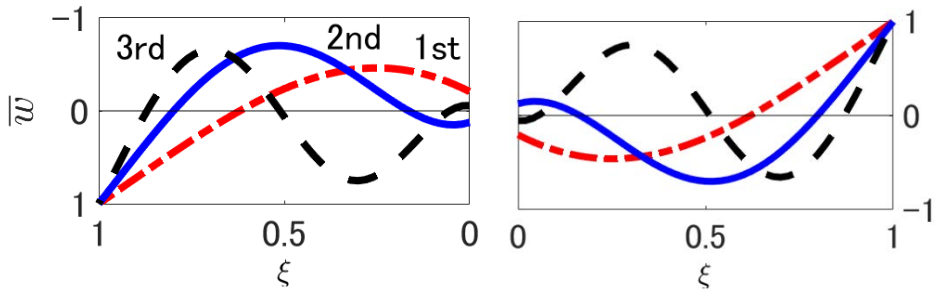

(a) $\overline{J}_t = 0.1$.

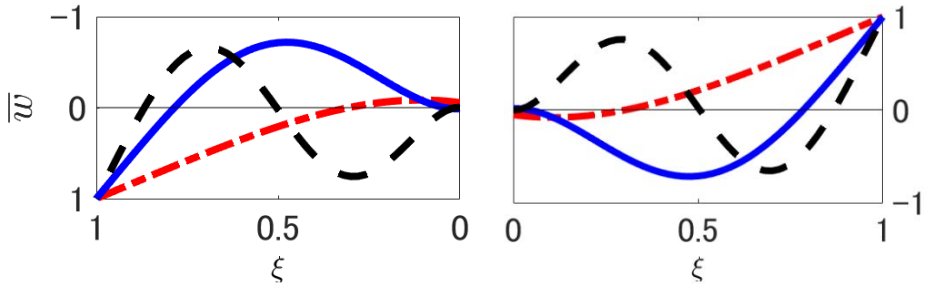

(b) $\overline{J}_t = 1$.

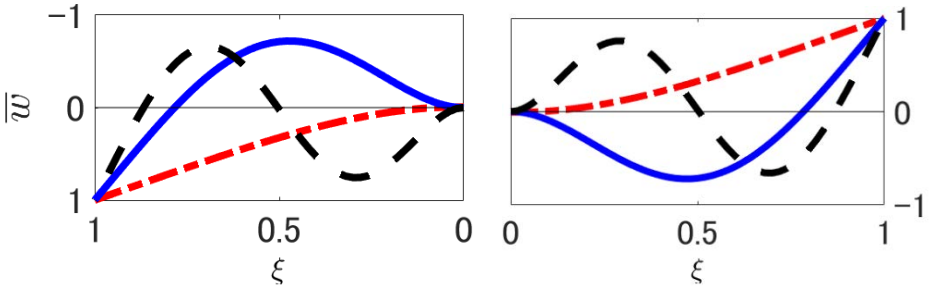

(c) $\overline{J}_t = 10$.

Fig. 4. Variations of vibration mode of elastic beams with inertia moment $\overline{J}_t$, $\lambda = 10$.; (a) $\overline{J}_t = 0.1$.; (b) $\overline{J}_t = 1$.; (c) $\overline{J}_t = 10$.

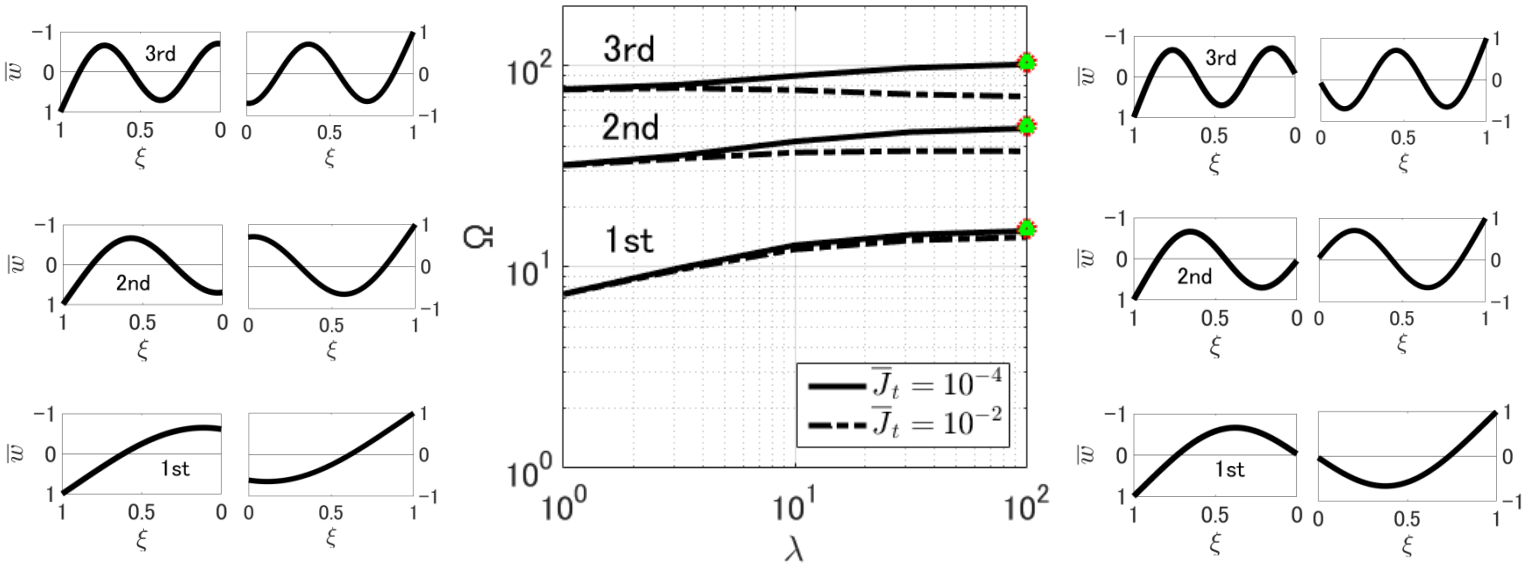

(b) $\lambda = 1,\ \bar{J}_t = 10^{-4}$. (a) Natural frequency with λ. (c) $\lambda = 100,\ \bar{J}_t = 10^{-4}$.

Fig. 5. Variations of natural frequency Ω and vibration mode with aspect ratio λ, $\bar{J}_t = 10^{-2}, 10^{-4}$.; (a) Natural frequency.; (b) $\lambda = 1,\ \bar{J}_t = 10^{-4}$.; (c) $\lambda = 100,\ \bar{J}_t = 10^{-4}$.

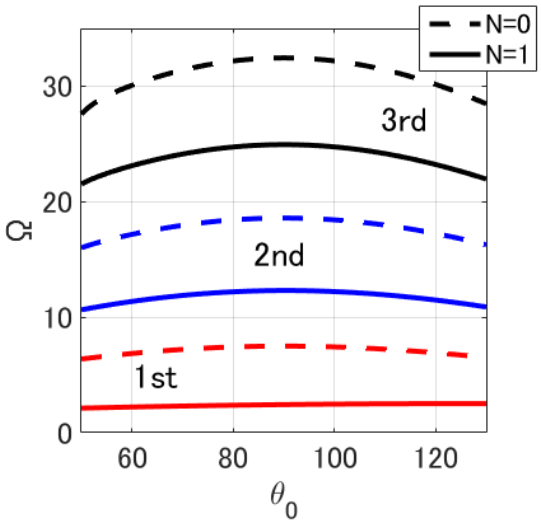

Fig. 6. Variations of natural frequency Ω with contact angle θ_0, N=0, 1, $h_0 = 1, \lambda = 1, \bar{\beta} = 1, \bar{\rho} = 1, \gamma = 1$.

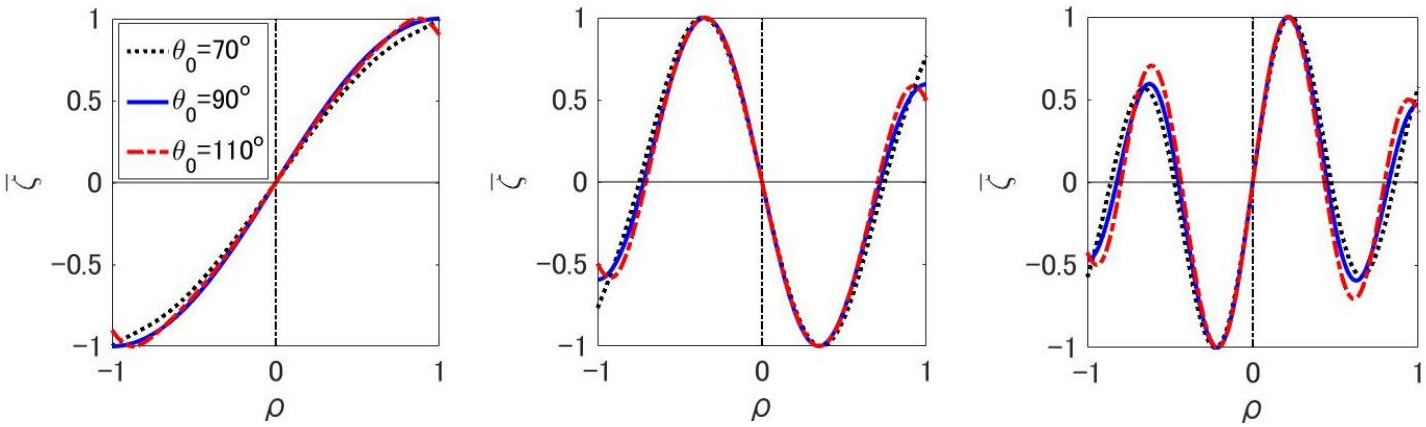

(a) 1st mode ($m=0$). (b) 2nd mode ($m=1$). (c) 3rd mode ($m=2$).

Fig. 7. Variations of free liquid free surface mode with contact angle θ_0, $h_0=1$, $\lambda=1$, $\bar{\beta}=1$, $\bar{\rho}=1$, $\gamma=1$, $N=1$.; (a) 1st mode ($m=0$).; (b) 2nd mode ($m=1$).; (c) 3rd mode ($m=2$).

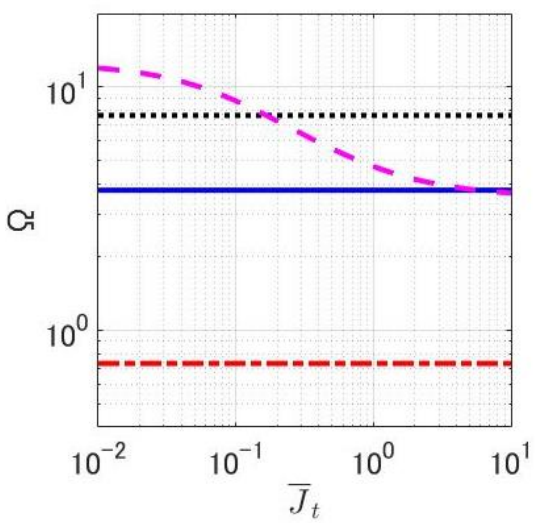

(a) Up to the 4th mode.

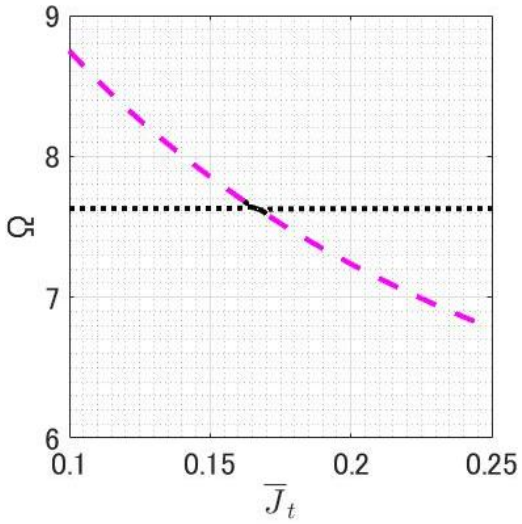

(b) Interaction between the 3rd and 4th frequency curves.

Fig. 8. Variations of natural frequency Ω with inertia moment $\overline{J}_t$, $\theta_0 = 70^\circ$, $\lambda = 10, h_0 = 1, \overline{\beta} = 10,\ \overline{\rho} = 1,\ \gamma = 10^{-4}, N = 1$.; (a) Up to the 4th mode.; (b) Interaction between the 3rd and 4th frequency curves.

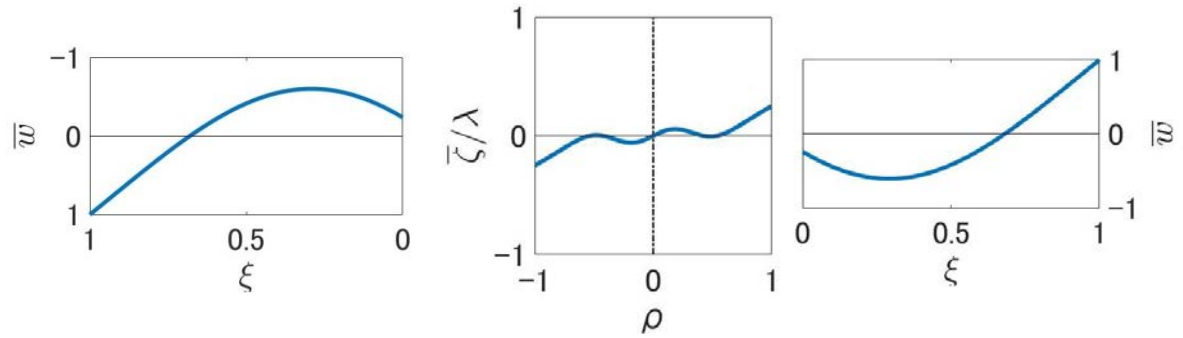

(a) $\overline{J}_t = 0.03$.

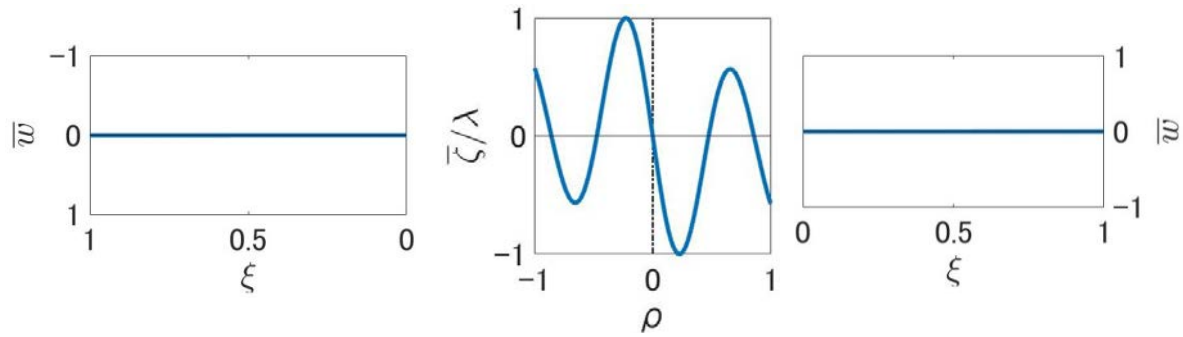

(b) $\overline{J}_t = 1.00$.

Fig. 9. Variations of vibration mode with inertia moment $\overline{J}_t$,
$\theta_0 = 70^\circ$, $\lambda = 10, h_0 = 1, \overline{\beta} = 10,\ \overline{\rho} = 1,\ \gamma = 10^{-4}, N = 1$.; (a) $\overline{J}_t = 0.03$.; (b) $\overline{J}_t = 1.00$.

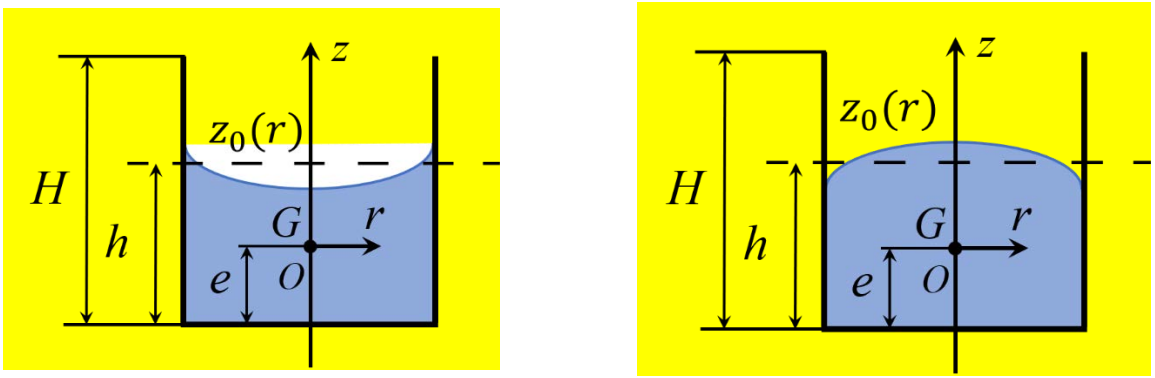

(a) $\theta_0 \le 90^\circ$ (b) $90^\circ \le \theta_0$

Fig. A1. Integration region depending contact angle θ_0 .;(a) $\theta_0 \le 90^\circ$;(b) $90^\circ \le \theta_0$.